

# 博士論文

## **Differential roles of annexins and ESCRTs in lysosome repair**

(リソソーム修復におけるアネキシンと ESCRT の異なる役割)

イン・ウィラ・ワン・ヨウ

**Yim Willa Wen You**

# **Differential roles of annexins and ESCRTs in lysosome repair**

Affiliation: Department of Biochemistry and Molecular Biology, Graduate School of  
Medicine, The University of Tokyo, Tokyo 113-0033, Japan

Supervisor: Noboru Mizushima

Yim Willa Wen You

## Contents

	Page
Abbreviations.....	3
Abstract.....	5
Introduction.....	6
Materials and Methods.....	13
Results.....	22
Discussion.....	48
References.....	56
Acknowledgements.....	66

## Abbreviations

A647: Alexa Fluor 647

ALG2: Apoptosis-linked gene 2

ALIX: ALG-2-interacting protein X

ANX: Annexin

ATP: Adenosine triphosphate

BAPTA-AM: 1,2-Bis(2-aminophenoxy)ethane-N,N,N',N'-tetraacetic acid  
tetrakis(acetoxymethyl ester)

BMP: Bis(monoacyl)glycerophosphate

BSA: Bovine serum albumin

CHMP: Charged multivesicular body protein

DMEM: Dulbecco's modified Eagle's medium

DMSO: Dimethyl sulfoxide

ESCRT: Endosomal sorting complexes required for transport

FITC: Fluorescein isothiocyanate

GFP: Green fluorescent protein

HEK: Human embryonic kidney cells

HRP: Horseradish peroxidase

HRS: Hepatocyte growth factor-regulated tyrosine kinase substrate

HSP70: Heat shock protein 70

HSP90: Heat shock protein 90

IQR: Interquartile range

LAMP1: Lysosomal-associated membrane protein 1

LIMP2: Lysosomal integral membrane protein 2

LLOMe: L-leucyl-L-leucine methyl ester

LRRK2: Leucine-rich repeat kinase 2

NA: Numerical aperture

PBS: Phosphate-buffered saline

PDCD6: Programmed cell death 6

PDCD6IP: Programmed cell death 6 interacting protein

siRNA: Small interfering RNA

SDS-PAGE: Sodium dodecyl sulfate-poly-acrylamide gel electrophoresis

SF650: HaloTag ligand SaraFluor 650T

SMPD: Sphingomyelin phosphodiesterase

STAM: Signal transducing adapter molecule 1

TBST: Tris-buffered saline with Tween-20

TMEM192: Transmembrane protein 192

TMR: Tetramethylrhodamine

TSG101: Tumor susceptibility gene 101

U2OS: U-2 osteosarcoma cells

VPS: Vacuolar protein sorting-related

## **Abstract**

To prevent the leakage of hydrolases from lysosomes, lysosomal membranes must be quickly repaired when damaged. Repair of the plasma membrane and the lysosomal membrane is initiated by calcium leakage into the cytosol, which recruits the membrane fission machinery, ESCRT. Plasma membrane repair also requires annexins (ANXs), which are a family of proteins that associate with membranes when bound to calcium and carry out a variety of membrane repairing mechanisms. However, the role of annexins in lysosome repair has not been clarified. Here, I show that all ubiquitously expressed annexins (ANXA1, A2, A4, A5, A6, A7, and A11) are recruited to damaged lysosomes. Among them, only ANXA1 and ANXA2 are important for lysosome repair. ANXA1 and ANXA2 localize to damaged lysosomes in a calcium-dependent manner, as do ESCRTs. Despite this similarity, ANXA1 and ANXA2 localize to only a subset of ESCRT-positive damaged lysosomes. I show that ANXA1 and ANXA2 are preferentially recruited to lysosomes with large membrane wounds that allow preloaded 10-kDa dextran to pass through. The leakage of 10-kDa dextran from lysosomes is exacerbated by depletion of ANXA1 or ANXA2. These findings indicate that ANXA1 and ANXA2 serve as an additional repair mechanism for lysosomes and that their primary function may be to minimize leakage from lysosomes with large membrane wounds.

## **Keywords**

Annexins, ESCRTs, lysosome repair, membrane damage, membrane repair

## Introduction

Lysosomes are the mammalian cell's degradative organelles. They recycle intracellular material and eliminate undesirable material such as pathogens and protein aggregates, and, in doing so, maintain cellular metabolism and homeostasis [1, 2]. Lysosomal function is contingent on the acidity of its lumen (pH ~4.5-5.5), which, in turn, requires the lysosomal membrane to be intact [1].

As sites of degradation, lysosomes encounter a wide range of substances, which includes membrane-destabilizing material. Endocytosed pathogens, amyloid-beta aggregates [3], alpha-synuclein aggregates [4], urate crystals [5-7], foreign microparticles and so on can disrupt the lysosomal membrane. Lysosomal membrane permeabilization can also result from the loss of membrane-stabilizing proteins (e.g., HSP70 [8], LIMP2 [9], and Myoferlin [10]) and from changes in lipid composition, such as aberrant levels of cholesterol [11-13] and higher levels of the single-tailed and thus detergent-like lipid sphingosine [14-16]. Chances of lysosomal membrane permeabilization increase with age and in diseases where aberrant material accumulates in lysosomes, such as neurodegenerative diseases and lysosomal storage diseases. Not all outcomes are undesirable—tightly regulated lysosomal membrane permeabilization has been proposed to have beneficial effects. For example, released cathepsins contribute to the regulation of chromosome segregation during mitosis and the regulation of cell adhesion structures during cell motility [17]. Unregulated lysosomal membrane permeabilization, on the other hand, is hazardous to the cell, with consequences of lysosomal membrane permeabilization ranging from inactivation (due to loss of acidity) to cell death (due to release of lysosomal hydrolases into the cytosol) [18, 19].

After damaged lysosomes were reported to be cleared by autophagy ('lysophagy') in 2012 [15], elimination was thought to be their only fate [20-24]. This view was expanded in

2018 by two reports of lysosome repair mediated by Endosomal Sorting Complexes Required for Transport proteins (ESCRTs) [25, 26]. Lysosome repair was made observable by reducing lysosomal exposure to damaging agent, thereby inducing a milder degree of lysosomal damage [25, 26] compared to that in previous studies on lysophagy [20-24]. How damaged lysosomes are resolved is now understood to depend on whether the inflicted damage is repairable. Since elimination leads to the loss of lysosomes, repair is the preferred outcome (Figure 1) [27].

Membrane repair is well-studied for the plasma membrane. Damage to the plasma membrane results in the influx of calcium from the extracellular space into the cytosol, which then recruits two major groups of proteins: ESCRTs and the annexins (ANXs) [28-32] (Figure 2A). There are at least 30 ESCRTs in mammalian cells that assemble on membrane sequentially. Most of what is known about ESCRT-mediated membrane deformation comes from studies on ESCRT-mediated intraluminal vesicle formation on late endosomes. During intraluminal vesicle formation, ESCRTs are sequentially recruited to proteins destined for the intraluminal vesicles, beginning with ESCRT-0 and ending with ESCRT-III. ESCRT-III proteins polymerize into filaments, forming a spiral structure that pushes the late endosomal membrane into the lumen. Eventually, a membrane bud is formed, with the ESCRT-III spiral concentrated at the neck connecting the membrane bud to the late endosomal membrane. At the same time, the ESCRT-III spiral undergoes remodeling by the AAA-ATPase VPS4, which removes ESCRT-III monomers for recycling. The energy generated by VPS4 also powers the ESCRT-III to constrict the bud neck, which results in the separation of the membrane bud (now referred to an intraluminal vesicle) from the late endosomal membrane [32-36] (a more detailed description can be found in the figure legend for Figure 3A). ESCRT-mediated membrane repair has been proposed to be achieved by the assembly of ESCRT-III spiral around the membrane wound—in the same manner as in intraluminal



vesicle formation—to create an ‘intraluminal vesicle’ that contains the membrane wound, thereby removing the wound from the previously damaged membrane [37] (Figure 3B).

In contrast to the sequential action of ESCRTs, annexins carry out different and sometimes multiple functions to repair membrane wounds on the plasma membrane [28-30]. Annexins are a family of 12 calcium-binding proteins that associate with membranes in a calcium-dependent manner. They are characterized by the presence of a highly conserved core domain consisting of four (eight for ANXA6) ~70 amino acid-long repeats that are individually capable of binding up to three calcium ions and, in turn, three phospholipid head groups [38] (Figure 3C). In contrast to the core domain, the N-terminal domain of each annexin is unique—varying in sequence and length—and differentiates the function of one annexin from another [38]. Of the 12 annexins, six have been shown to be important to plasma membrane repair: ANXA1 [39-41], A2 [39, 42-44], A4 [45], A5 [46, 47], A6 [45, 48, 49], and A7 [50]. They may promote membrane repair by forming membrane arrays to stabilize the membrane wound (ANXA5) [46], by forming oligomers that cap the wound (ANXA1, A2, A5, A6) [41, 47, 49], by constricting the wound edges to promote sealing (ANXA4, A6) [45] or by aggregating endosomes or lysosomes to patch the wound (ANXA1, A2) [39, 40, 48] (Figure 3D). Furthermore, ANXA7 serves as the upstream factor recruiting ESCRTs, which do not have calcium-binding domains, to plasma membrane injuries [50] (Figure 2A). With distinctive mechanisms, annexins and ESCRTs work alongside each other to repair the plasma membrane when it is damaged.

Despite their prominence in plasma membrane repair, whether annexins are involved in lysosome repair has yet to be fully explored. Given that lysosome repair and plasma membrane repair are both triggered by calcium influx through the membrane wounds [25, 26, 51-53] (Figure 2), they might share calcium-dependent repair mechanisms other than ESCRTs. Hints of annexin involvement in lysosome repair can be found in previous studies:

a 2012 study reporting the localization of ANXA2 to lysosomes destabilized by wear debris [54] and the proteomics-based detection of annexins among the proteins found in increased levels in damaged lysosomes [55, 56]. However, whether annexins are important for lysosome repair and, if found to be so, the relationship between annexins and ESCRTs in lysosome repair have not been addressed.

In this study, I show that although all ubiquitously expressed annexins (ANXA1, A2, A4, A5, A6, A7, and A11) localize to damaged lysosomes, only ANXA1 and ANXA2 are required for the efficient repair of lysosomes. While ESCRTs are recruited to most damaged lysosomes, ANXA1 and ANXA2 are preferentially recruited to damaged lysosomes with larger membrane wounds to prevent excessive leakage of lysosomal contents—a function that is independent of ESCRTs but important for efficient repair.

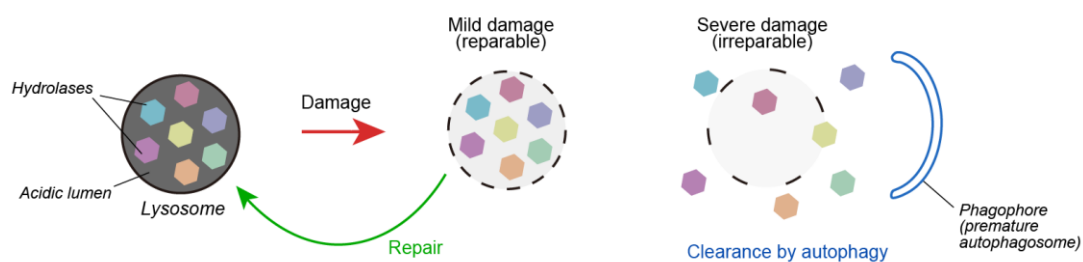


**Figure 1. Fate of damaged lysosomes depends on damage severity.**

Pathogens, protein aggregates, uric acid crystals and so on can cause lysosomal membrane permeabilization. Damage is repaired whenever possible but when the extent of damage exceeds repair capabilities, the lysosome is eliminated by autophagy ('lysophagy').

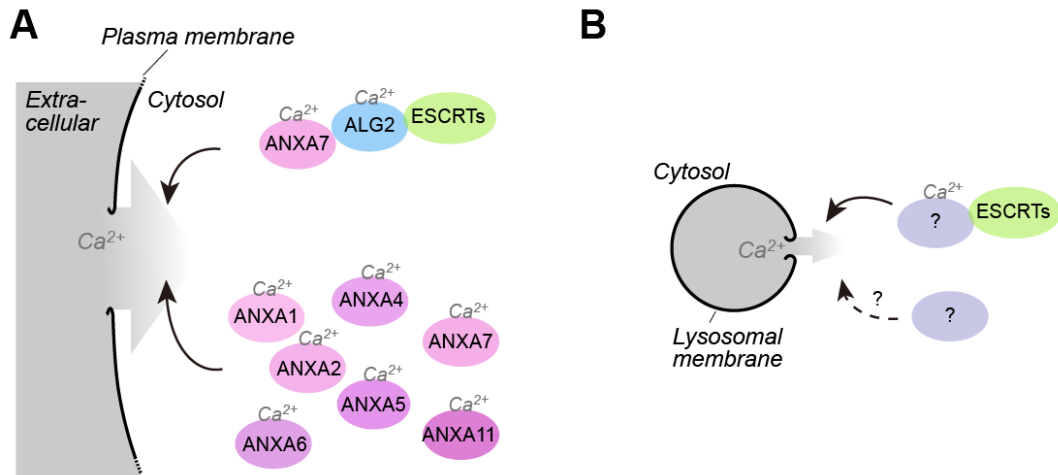


**Figure 2. Repair mechanisms for the plasma membrane and lysosomal membrane.**

**(A)** Disruptions in the plasma membrane allows calcium to enter the cytosol from the extracellular space. The local elevated calcium levels at the injury site recruits repair proteins. In the case of plasma membrane repair, annexins (ANXs) with calcium-binding domains can be recruited directly to plasma membrane injuries. After binding to calcium, annexins undergo a conformational change that allows them to associate with membrane. ANXA1, A2, A4, A5, A6, and A7 have been individually shown to mediate plasma membrane repair. Furthermore, ANXA7 binds to ALG2, which in turn recruits the ESCRT machinery (consisting of at least 30 proteins in mammalian cells) to the plasma membrane wound. ESCRTs then mediate wound resealing. **(B)** Lysosome damage also leads to release of calcium into the cytosol. The increased calcium levels around the membrane wound in the lysosomal membrane recruits ESCRTs, which then mediate repair. Whether annexins are involved to directly repair lysosomes or to help recruit ESCRTs to the calcium-rich wounds on lysosomes have not been clarified.

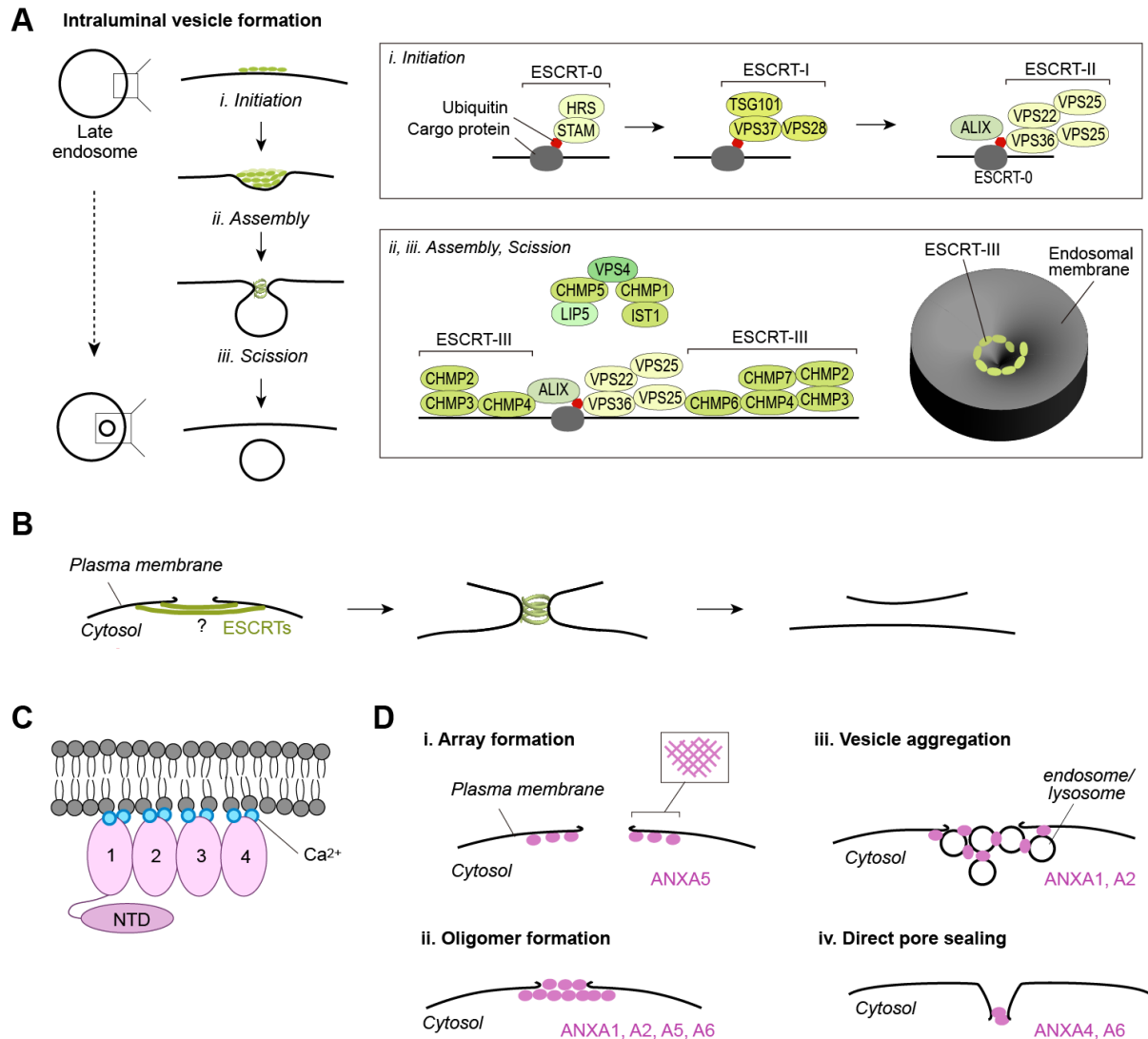


**Figure 3. Models for membrane repair mediated by ESCRTs and annexins.**

(A) ESCRT membrane activity is best studied in the context of intraluminal vesicle formation on late endosomes. (i) ESCRT-0 proteins, HRS and STAM, are recruited to typically ubiquitinated cargo proteins to arrange them into clusters. ESCRT-I proteins, TSG101, VPS28, and VPS37, are then recruited to the assembly site. VPS22, VPS25, and VPS36 constitute ESCRT-II and are recruited by ESCRT-I. ALIX (PDCD6IP) is recruited independently of ESCRT-I as it contains binding domains for ubiquitin and bis(monoacyl)glycerophosphate (BMP), which is a lipid characteristic of late endosomes. (ii, iii) ESCRT-II and ALIX interact separately with components of ESCRT-III (CHMP1-6, and IST1) to recruit them to the assembly site. ESCRT-III proteins polymerize into filaments that circle on the endosomal membrane, pushing it downwards to the lumen (see the 3D model). The AAA-ATPase VPS4 is recruited to the ESCRT-III filaments via interactions with CHMP5, CHMP1, and/or IST1. Powered by ATP, VPS4 removes ESCRT-III monomers from the ESCRT-III filaments for recycling. Eventually, a membrane bud is formed, with the ESCRT-III spiral at the connection between the bud and the late endosomal membrane. ESCRT-III filaments then constrict to result in scission of the bud neck in an ATP- and thus VPS4-dependent manner. The membrane bud is released into the late endosomal lumen as an intraluminal vesicle. (B) The model for ESCRT-mediated membrane repair is based on the mechanism of ESCRT-mediated intraluminal vesicle formation on late endosomes (A). The ESCRT-III spiral is proposed to form around the plasma membrane wound, inducing budding and eventual excision of the membrane area containing the wound. How the spiral would form around the membrane injury is unknown. (C) Annexins are proteins with a core composed of four (eight

in the case of ANXA6) calcium-binding and lipid-binding repeats. Their function is dictated by their N-terminal domains, which differentiate the annexins from each other. **(D)** In addition to ANXA7 recruiting ESCRTs to plasma membranes, there are various membrane repair mechanisms by annexins that are independent of ESCRT activity. (i) ANXA5 were observed to form structured arrays *in vitro* and thus proposed to assemble into arrays around the plasma membrane wound to prevent it from expanding. (ii) ANXA1, A2, A5, and A6 were observed to form a cap over plasma membrane wounds. (iii) ANXA1 and ANXA2 are known to induce membrane aggregation, which is thought to promote lysosome and endosome-containing patch formation over the membrane wound. (iv) ANXA4 and ANXA6 were also shown to constrict wound edges to promote sealing.

## **Materials and Methods**

### **Cell culture**

Cells were maintained in a 37°C, 5% CO<sub>2</sub> incubator. Authenticated U2OS human osteosarcoma and human embryonic kidney (HEK) 293 cell lines were used in this study. They were grown in Dulbecco's modified Eagle's medium (DMEM; D6546; Sigma-Aldrich), supplemented with 10% FBS (173012; Sigma-Aldrich) and 2 mM L-glutamine (25030-081; Gibco).

### **Antibodies**

Primary antibodies that were used for immunoblotting are: anti-ANXA1, anti-ANXA2 (66035-1-IG; Proteintech), anti-ANXA6 (sc-271859; Santa Cruz Biotechnology), anti-ANXA7 (10154-2-AP), anti-ANXA11 (sc-46686; Santa Cruz Biotechnology), anti-TSG101 (GTX70255; Genetex), anti-ALIX (634502; Biolegend), anti-ALG2/PDCD6 (12303-1-AP; Proteintech), anti-HSP90 (610419; BD Transduction Laboratories). Secondary antibodies conjugated with horseradish peroxidase that were used for immunoblotting are as listed: anti-mouse (111-035-003; Jackson ImmunoResearch Laboratories) and anti-rabbit (111-035-144; Jackson ImmunoResearch Laboratories). Primary antibodies that were used for immunostaining are as listed: anti-ALIX (634502; Biolegend), anti-CHMP4B (13683-1-AP; Proteintech), anti-ALG2/PDCD6 (12303-1-AP; Proteintech), anti-LAMP1 (ab24170; Abcam), anti-Galectin-3 (125402; BioLegend). Secondary antibodies that were used for immunostaining are as listed: Alexa Fluor 488-conjugated anti-mouse IgG (A11008; Thermo Fisher Scientific), Alexa Fluor 568-conjugated anti-rabbit IgG (A11011; Thermo Fisher Scientific), and Alexa Fluor 660-conjugated anti-rat IgG (A21247; Thermo Fisher Scientific).

## Plasmid constructs

cDNAs encoding human *ANXA1* (NM\_000700.3), *ANXA2* (NM\_001002858.3), *ANXA4* (NM\_001320698.2), *ANXA5* (NM\_001154.4), *ANXA6* (NM\_001155.5), *ANXA7* (NM\_001156.5), and *ANXA11* (XM\_005269741.4) were amplified from total cDNA obtained from HEK 293 cells. They were inserted into pMRX-IZU (a plasmid generated from pMXS but with zeocin marker) with either mRuby3 at the N-terminus or at the C-terminus. CHMP4A was inserted into a pMRX-IBU (a plasmid generated from pMXS with blasticidin marker) with HaloTag (Promega) at the N-terminus.

Appli- cation	Target gene	Forward primer sequence	Reverse primer sequence
Cloning	ANXA1	CATGGGATCCATGGCAATGGTATCAGAA TTCCTC	ATGAGGATCCGTTTCCTCCACAAAGAGCCA CC
Cloning	ANXA2	ATTCGGATCCATGGGCCGCCAGCTAGCG GGGTG	ATCTGGATCCGTCATCTCCACCACACAGGT AC
Cloning	ANXA4	ATCTGGATCCATGGCCATGGCAACCAAA GGAGG	ATCTGGATCCTTAATCATCTCCTCCACAGA GAACAAG
Cloning	ANXA5	ATGAAAGCTTATGGCACAGGTTCTCAGA GGCAC	ATAGAAGCTTGTCTCTCTCCACAGAGCA GC
Cloning	ANXA6	TATGAAGCTTATGGCCAAACCAGCACAG GGTG	ATAGAAGCTTGTCTCTCACCACCACAGAGAG CC
Cloning	ANXA7	ATCTGGATCCATGTCATACCCAGGCTATC CCCCAA	ATCTGGATCCCTGGCCACAATAGCCAGA AG
Cloning	ANXA11	ATCTGGATCCATGGTGTCCACAACAGT CTG	ATCTGGATCCGTCATTGCCACCACAGATCT TC
Cloning	CHMP4A	ATGAGTGGTCTCGGCAGGCTCTT	GGATACCCACTCAGCCAACTGC
qPCR	ANXA4	ACGGAGCCTTGAAGATGACA	TCCTGTCTCACGAGAGCATC
qPCR	ANXA5	CAGGTTCTCAGAGGCACTGT	CTCTCCTCATCTGTGCCCAA

**Table 1. Primer sequences.**

## Retrovirus production and transduction.

At 60% confluency, HEK293T cells in a 3.5 cm dish were transiently transfected with 1.8 µg retroviral vector carrying the gene of interest, 0.9 µg pCG-VSV-G, 0.9 µg pCG-gag-pol (gifts from Dr. T. Yasui, National Institutes of Biomedical Innovation, Health and Nutrition), and 2 µl Lipofectamine 2000 (11668019; Thermo Fisher Scientific). The DNA mixture and Lipofectamine mixture were incubated separately for 5 min before being mixed

and incubated for another 10 min at room temperature. The final volume of medium was 1.5 ml OPTI-MEM (31985070; Thermo Fisher Scientific). The medium was replaced with DMEM after 16 h. After 24 h, the medium was collected, centrifuged at  $2500 \times g$  for 3 min, and passed through a 0.45- $\mu$ m syringe filter unit (SLHV033RB; EMD Millipore). Before transduction, DMEM was added to the retrovirus-containing medium at a 1:3 ratio. The mixture was then added to U2OS cells with 8  $\mu$ g/mL polybrene (H9268; Sigma-Aldrich). Stable transformants were selected with 2  $\mu$ g/ml puromycin (P8833; Sigma-Aldrich), 3  $\mu$ g/ml blasticidin (022-18713; Wako Pure Chemical Industries), or 2.5  $\mu$ g/ml zeocin (R25005; Thermo Fisher Scientific).

### **RNA interference**

Silencer Select siRNA (Thermo Fisher Scientific) was used and the product IDs can be found in Table 2. siRNA transfection was conducted with Lipofectamine RNAiMAX (13778150; Thermo Fisher Scientific) in a 12-well plate format. 15 nM of siRNA was prepared in OPTI-MEM with RNAiMAX before being added to a single well of cells to a final mixture of 20% OPTI-MEM and 80% DMEM. The medium was changed 24 h after transfection. Imaging or protein collection was carried out after another 24 h.

### **RNA extraction and quantitative PCR**

Total RNA was extracted from cells using Isogen (319-90211; Nippon Gene). Reverse transcription was carried out using Rivergrade (FSQ-201; TOYOBO) as per manufacturer's instructions. Samples were prepared in triplicate with TB Green Premix Ex Taq II (RR820, TaKaRa Bio Inc) and underwent PCR in a Thermal Cycler Dice TP800 (TaKaRa Bio Inc).



Target gene	Target RefSeq	siRNA ID
ALIX	NM_013374	s19465
TSG101	NM_006292	s14439
PDCD6	NM_013232	s19469
ANXA1	NM_000700	1380
ANXA1	NM_000700	1381
ANXA2	NM_004039	s1384
ANXA2	NM_004039	s1385
ANXA4	NM_001153	s1389
ANXA4	NM_001153	s1390
ANXA5	NM_001154	s1392
ANXA5	NM_001154	s1393
ANXA6	NM_001155	1396
ANXA6	NM_001155	1397
ANXA7	NM_004034	s1398
ANXA7	NM_004034	s1399
ANXA11	NM_145869	s1402
ANXA11	NM_145869	s1401

**Table 2. The product IDs of siRNAs used in this study.**

## Immunoblotting

Cells were lysed with ice-cold lysis buffer (50 mM Tris-HCl (pH 7.4), 150 mM NaCl, 1 mM EDTA, 1% Triton X-100, and complete EDTA-free protease inhibitor cocktail (19543200; Roche)). The cell suspension was centrifuged at  $12,000 \times g$  for 10 min and the supernatant was collected. Protein concentration was determined using the Bradford protein assay (5000006JA; Bio-Rad). The protein concentration was then mixed with sample loading buffer (46.7 mM Tris- HCl, pH 6.8, 5% glycerol, 1.67% sodium dodecyl sulfate, 1.55% dithiothreitol, and 0.02% bromophenol blue) and stored at  $-20^{\circ}\text{C}$  or incubated at  $95^{\circ}\text{C}$  for 5 min if to be subjected to SDS-PAGE immediately after. After SDS-PAGE, samples were transferred onto a piece of Immobilon-P polyvinylidene difluoride membrane (IPVH00010; EMD Millipore). The membrane is first incubated in 5% skimmed milk in Tris-Buffered Saline with Tween 20 (TBST; 20 mM Tris-Cl, 150 mM NaCl, 0.1% (w/v) Tween 20 (02194841-CF; MP Biomedicals)) for 30 min at room temperature, the primary antibody in

2.5% skimmed milk in TBST for 1 h at room temperature (or for 16 h at 4°C), and the secondary antibody in 2.5% skimmed milk in TBST for 1 h at room temperature. The membrane was washed with TBST three times for 5 min each between the two antibodies and after the secondary antibody. Immobilon Western Chemiluminescent HRP Substrate (P90715; EMD Millipore) was applied to the membrane to visualize the signals on the Fusion System Solo 7S (M&S Instruments). The color of the signals was inverted using Fiji [57]. No other adjustments to the signal were made.

### **Immunostaining**

Cells were grown on coverslips in a 24-well plate and after incubating with 1 mM LLOMe (L7393; Sigma) for the desired period of time, they were washed with PBS and fixed with 4% paraformaldehyde in PBS (09154-85; Nacalai Tesque) for 10 min at room temperature. After 3 PBS washes, they were permeabilized with 50 µg/mL digitonin (D141; Sigma-Aldrich) in PBS for 5 min, washed with PBS twice and incubated with 3% bovine serum albumin (BSA; 011-27055; Wako) in PBS for 30 min. They were transferred from the 24-well plate to a shallow, cling film-covered container, with the side covered by cells facing upwards. The primary antibody in 3% BSA was applied to the coverslip and this was left at room temperature for 1 h or at 4°C for 16 h. After four PBS washes, cells were applied with the appropriate Alexa Fluor-conjugated secondary antibodies for 1 h at room temperature. After three PBS washes, the coverslips were mounted onto glass slides with ProLong Gold Antifade Mountant (P36930; Thermo Fisher Scientific). When 405 nm fluorophores were not necessary, samples were stained with Hoechst33342 (H341; Dojindo Molecular Technologies) by covering the coverslip with 0.5 µg/mL Hoescht33342 in PBS for 5 min at room temperature before mounting.

## **Fluorescence microscopy**

Fluorescence microscopy was performed on a confocal laser microscope (FV3000 IX81; Olympus) with a 60× oil-immersion objective lens (1.40 NA; Olympus) and captured with FluoView software (Olympus). All image analyses were conducted using Fiji with ImageJ macros [57]. Puncta quantification was conducted individually for each cell, where any signal above a predetermined percentile threshold were considered as puncta. These were then counted with the “Analyze Particles” function.

## **Live-cell microscopy**

All live-cell imaging was performed with the Olympus SpinSR10 spinning-disk confocal super-resolution microscope equipped with a Hamamatsu ORCA-Flash 4.0 camera, a UPLAPO OHR 60×/1.50 lens, and the SORA disk in place. The microscope was operated with Olympus cellSens Dimension v2.3. During imaging, cells were kept in a stage-top incubator (Tokai Hit) supplied with 5% CO<sub>2</sub> and kept at 37°C. The imaging medium used was FluoroBrite DMEM (A1896701; Thermo Fisher Scientific) supplemented with 10% FBS, 2 mM glutamine (Gibco, 25030-081), 50 U/ml penicillin and 50 µg/ml streptomycin (Gibco, 15070-063).

ANXA1 and ANXA2 signals in live-cell imaging experiments were from transient transfection for a lower cytosolic background signal (unless otherwise stated in the figure legends). Transient transfection was performed with Fugene HD (VPE2311; Promega) was added to plasmid in a 3:1 ratio (3 µl:1 µg) in a mixture with 20% OPTI-MEM. The medium was replaced with DMEM 24 h later and imaging was conducted another 24-48 h later.

The concentration and incubation durations of LLOMe (L7393; Sigma Aldrich) treatment are indicated in the figure legends. The dextrans used in this study are: 10K-dextran conjugated to Alexa Fluor 647 (D22914; Thermo Fisher Scientific), and 40K-dextran

conjugated to fluorescein isothiocyanate (FITC; D1845; Thermo Fisher Scientific). Cells were incubated with 25  $\mu$ g/ml dextran in DMEM for 12-16 h, following which dextran-containing DMEM was replaced with regular DMEM after two washes with PBS. Imaging was carried out after 2-4 h of incubation with DMEM ('chase'), during which all dextran molecules would have reached the lysosomes.

For experiments with BAPTA-AM, cells were incubated in imaging medium with 0.1 mM BAPTA-AM (03731-24; Nacalai) for 1 h before imaging and during imaging. Quantification of ANXA1 and CHMP4A signal was conducted on raw images with Fiji [57], using suitable percentile thresholds to detect signals and "Analyze Particles" to measure their area.

Classifying lysosomes as '10K-dextran positive' or '10K-dextran negative' (Figure 14) was achieved by first obtaining a threshold for the 10K-dextran channel using images taken before exposure to LLOMe. This threshold was then applied to the 10K-dextran images, resulting in binarized 10K-dextran signals. TMEM192-GFP positive ROIs were detected and those that overlapped with binarized 10K-dextran signals were classified as '10K-positive' and those that did not were classified as '10K-negative'. Both '10K-positive' and '10K-negative' sets of ROIs were then overlapped with the binarized ANXA1/A2 or CHMP4A channel to further classify them as ROIs positive or negative for ANXA1/A2 or CHMP4A signal. The classified ROIs were then counted with "Analyze Particles". This procedure was conducted for the image taken before LLOME addition and 16 min after LLOME addition for each cell individually.

Quantification of fluorescent signals of individual lysosomes (Figure 15) was carried out on raw images in Fiji [57]. Lysosomes were first tracked using the various markers, FITC-conjugated 40K-Dextran, HaloTag-CHMP4A and ANXA1-mRuby3. For each lysosome, a circular ROI was drawn around it for each time frame. The intensity values

within the ROIs were then measured and subsequently normalized by dividing each value by the average value of the ROIs taken before LLOMe exposure, following which the average value of the ROIs taken before LLOMe treatment was subtracted.

### **Magic Red recovery assay (live-cell fluorescence microscopy)**

The microscopy setup described in the ‘Live-cell microscopy’ section was used. Magic Red (ICT941; Bio-Rad Laboratories) was reconstituted in 50  $\mu$ l of DMSO and stored in 6  $\mu$ l aliquots at -20°C. It was diluted 1/2000 in imaging medium prior to imaging. 250  $\mu$ l of imaging medium was added to cells in one chamber of a 4-chamber glass-bottom dish (Greiner Bio). The fluorescence intensity of Magic Red fluorescence was allowed to stabilize for 10 min before starting the experiment. Six locations were chosen based on the uniformity of Magic Red fluorescence. Images were captured every 30 s for 5 time points. 250  $\mu$ l of imaging medium with LLOMe was added to give a final concentration of 0.3 mM. Two time points were acquired during LLOMe exposure. 1.5 min after the addition of LLOMe, imaging was paused for 1.5 min for the removal of the LLOMe-containing medium, two washes with imaging medium, and the addition of 750  $\mu$ l of imaging medium. Imaging was resumed and left to proceed uninterrupted for 25 min at 30 s intervals.

All image analyses were conducted on raw images using Fiji [57]. Cells were processed individually. The first of the five time points taken before LLOMe addition was discarded as the fluorescence signal of this time point tended to vary considerably from the next four timepoints. Lysosome signal (Magic Red or dextran) in each frame was detected by first obtaining a threshold that is the average of that detected using the “AutoThreshold” function on “MaxEntropy” setting of four frames prior to LLOMe addition. Fluorescence intensity values above the threshold was measured for each time point. The average value of

the four timepoints (taken before LLOMe treatment) was used to normalize all subsequent timepoints.

### **Dextran release assay (live-cell fluorescence microscopy)**

Cells were incubated with 25  $\mu$ g/ml of 10K-dextran in DMEM for 12-16 h. Imaging was carried 2-4 h after replacing the dextran-containing medium with regular DMEM. Images were taken as described for the Magic Red recovery assay, except with an interval of 1 min instead of 30 s. Quantification of dextran fluorescence was achieved with the same method as in the Magic Red assay except that a 97.5% percentile threshold was used to detect dextran signal.

### **Statistical analysis**

Statistical analyses were performed in *R*. The statistical methods used can be found in the relevant figure legends.

## Results

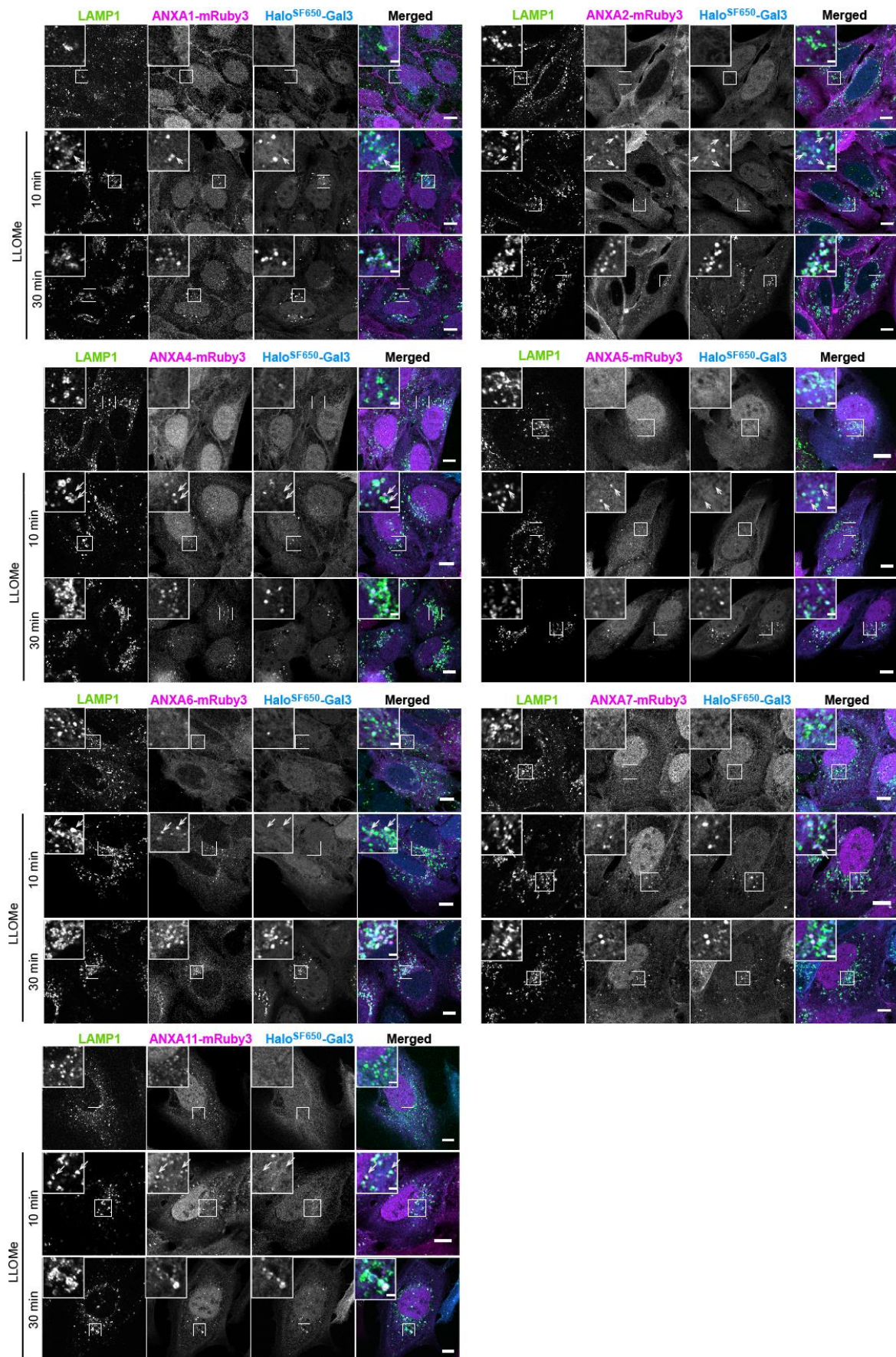
### *Annexins respond to lysosome damage*

To determine whether annexins are involved in lysosome repair, I examined the localization of the ubiquitously expressed annexins, ANXA1, A2, A4, A5, A6, A7, and A11 [58] (referred to as “annexins” collectively hereafter) before and after inducing lysosome damage. For visualization, the annexins were C-terminally tagged with mRuby3 (an N-terminal tag is not appropriate since the N-terminus of annexins are important to their function [38, 58]). Lysosomal damage was induced with the commonly used lysosomal membrane disrupting agent LLOMe (L-leucyl-L-leucine O-methyl ester) [18, 20, 25, 26, 53, 55], which is processed into membranolytic polymers by cathepsin C in lysosomes [59, 60]. LLOMe was previously shown to induce lysosome damage that requires clearance by lysophagy (i.e., the damage is beyond repair) after 30 min of incubation [26, 53, 55]. To capture annexin localization that may occur before lysophagy induction, their localization was imaged without and at 10 or 30 min of LLOMe incubation.

Annexins were cytosolic under normal conditions but, after 10 min of incubation with LLOMe, appeared as puncta that colocalized with 5–10% of structures positive for the lysosomal membrane protein LAMP1, representing lysosomes (Figure 4), indicating that they can respond to lysosome damage. Galectin-3 is a cytosolic protein that binds to the layer of glycosylation covering the luminal side of lysosomal membranes. Some annexin-positive lysosomes without galectin-3, which was visualized by tagging with HaloTag, could also be observed (Figure 4), suggesting that annexins can localize to mildly damaged lysosomes before they acquire membrane wounds large enough for proteins like galectins to pass through, which was also previously shown for ESCRTs [25, 26]. The number of annexin puncta increased after 30 min of incubation for all annexins except ANXA5 and ANXA6.

These data indicate that annexins are recruited to damaged lysosomes and might have varying levels of sensitivity to lysosome damage.





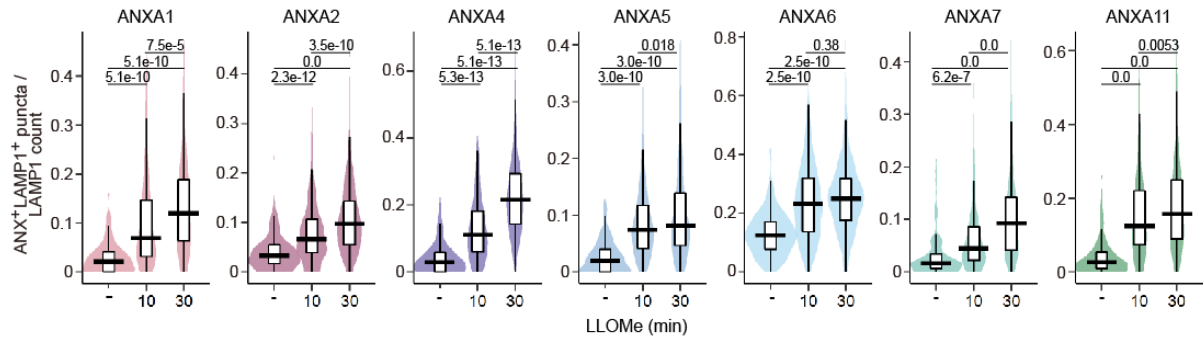


**Figure 4. Ubiquitously expressed annexins are recruited in the earlier stages of LLOMe-induced lysosome damage.**

U2OS cells expressing HaloTag-galectin3 (Gal3) were transduced with ANXA1-mRuby3, ANXA2-mRuby3, ANXA4-mRuby3, ANXA5-mRuby3, ANXA6-mRuby3, ANXA7-mRuby3, or ANXA11-mRuby3. Halo-Galectin3 was labeled with SaraFluor 650T (SF650) before the cells were treated with 1 mM LLOMe for 10 or 30 min or not at all. The cells were then fixed and stained with anti-LAMP1 antibody. Arrows point to annexin puncta that were negative for galectin-3. Data are shown with violin plots and boxplots, where the box spans the interquartile range (IQR) and the whiskers marking the within 1.5 IQR of the upper and lower quartiles.  $n = 150\text{--}332$  cells from 2 independent experiments. Statistical comparisons were conducted with one-way ANOVA and Tukey's Honestly Significant Difference test;  $p$  values as indicated.

***ANXA1 and ANXA2 are important for efficient lysosome repair.***

Next, to investigate whether annexins are important for lysosome repair, I employed the previously established Magic Red lysosome repair assay [25]. Magic Red is a chemical that fluoresces after being cleaved by lysosomal cathepsins, which allows it to specifically label functional lysosomes. Lysosomal membrane permeabilization causes Magic Red to dissipate from lysosomes that are now no longer acidic and without cathepsin activity to process Magic Red. Damaged lysosomes are thus Magic Red-negative. Successful lysosome repair restores lysosomal membrane integrity and acidity, allowing them to become Magic Red-positive again. Whether lysosomes are repaired can thus be determined from the recovery of Magic Red fluorescence after inducing mild lysosomal membrane permeabilization by briefly exposing cells to LLOMe [25, 61, 62] (Figure 5A).

After a 1.5 min brief exposure to 0.3 mM LLOMe, most lysosomes lost Magic Red signal, as seen from a decrease in overall Magic Red fluorescence (Figure 5B), which indicates that most lysosomes were damaged under this condition. LLOMe was then removed to allow lysosome repair. During washout, the lysosomes in cells transfected with negative control siRNA regained Magic Red fluorescence after around 20 min (Figure 5B), reflecting successful lysosome repair. By contrast, as previously reported [25], Magic Red fluorescence was not restored during washout in cells depleted of ALIX and TSG101 (Figure 5B), which recruit ESCRT-III to carry out membrane scission (Figure 3A).

Of the seven annexins tested, the depletion of ANXA1 or ANXA2 suppressed Magic Red recovery to a similar extent of ALIX-TSG101 double depletion (Figure 5B; Figure 6 for siRNA efficiency), indicating that ANXA1 and ANXA2 are both involved in lysosome repair. Furthermore, depleting ANXA1 and ANXA2 together did not cause additive suppression of Magic Red recovery (Figure 5B), suggesting that they share the same mechanism for lysosome repair.



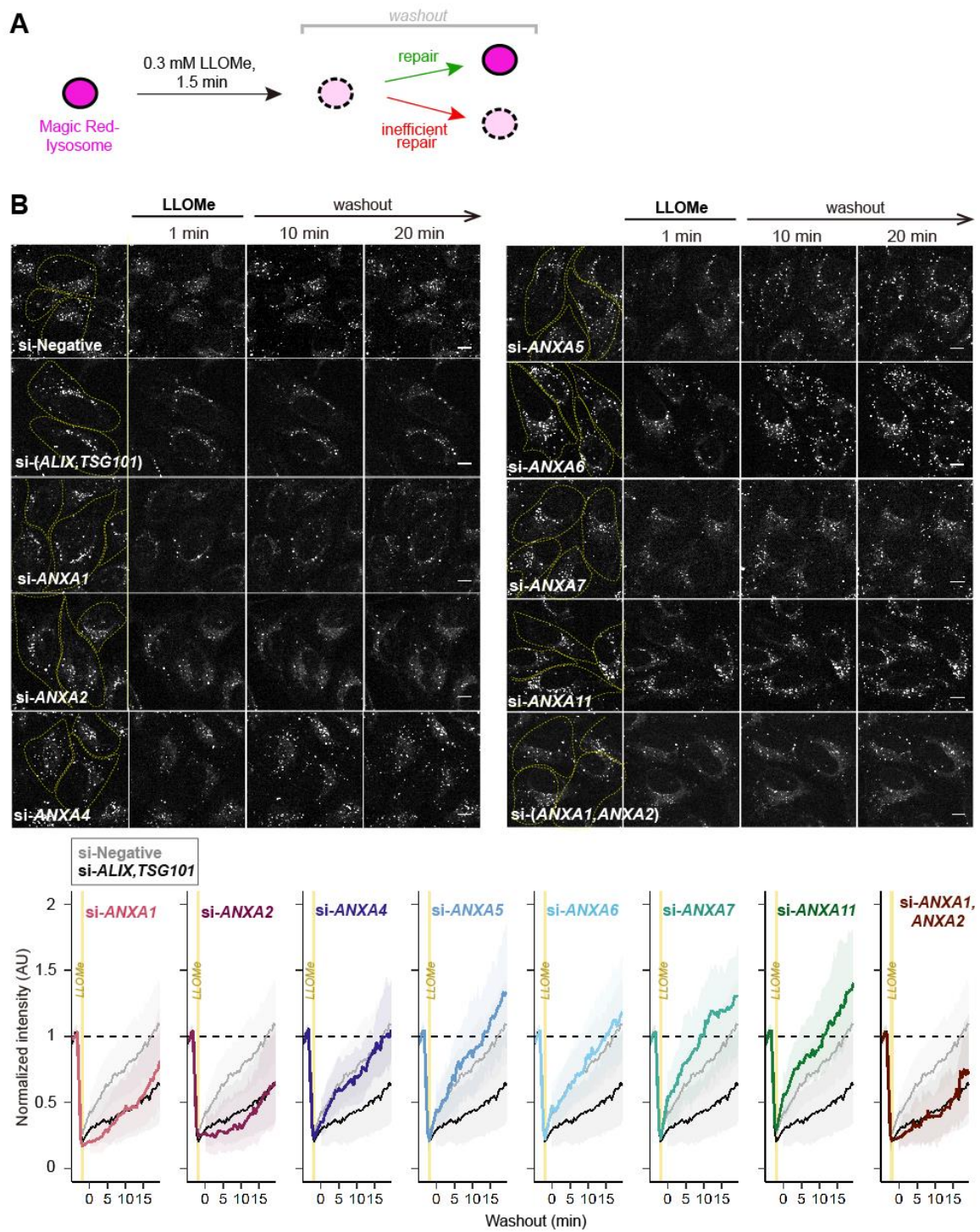


**Figure 5. Of the seven ubiquitously expressed annexins, depletion of ANXA1 or ANXA2 suppressed efficient lysosome repair.**

(A) Illustration of the changes in cathepsin activity indicator Magic Red fluorescence undergo in response to LLOMe-induced lysosome damage. Damaged lysosomes will become Magic Red-negative and regain Magic Red fluorescence after being repaired. (B) U2OS cells were transfected with the indicated siRNAs 72 h before imaging. After a 10 min pre-incubation with Magic Red, images of Magic Red fluorescence were captured at 30 s intervals before a 1.5 min incubation with 0.3 mM LLOMe and after ('washout'). The changes in Magic Red fluorescence

intensity over time was quantified for each cell and normalized to the average intensity of the 4 timepoints taken before LLOMe treatment. In the plots, lines trace the median values while the ribbons mark the 25<sup>th</sup> and 75<sup>th</sup> percentiles.  $n = 126\text{--}477$  cells from 3 independent experiments, except for si-*ANXA1*, *ANXA2* whose measurements were obtained from 2 independent experiments. Scale bar = 10  $\mu\text{m}$ .

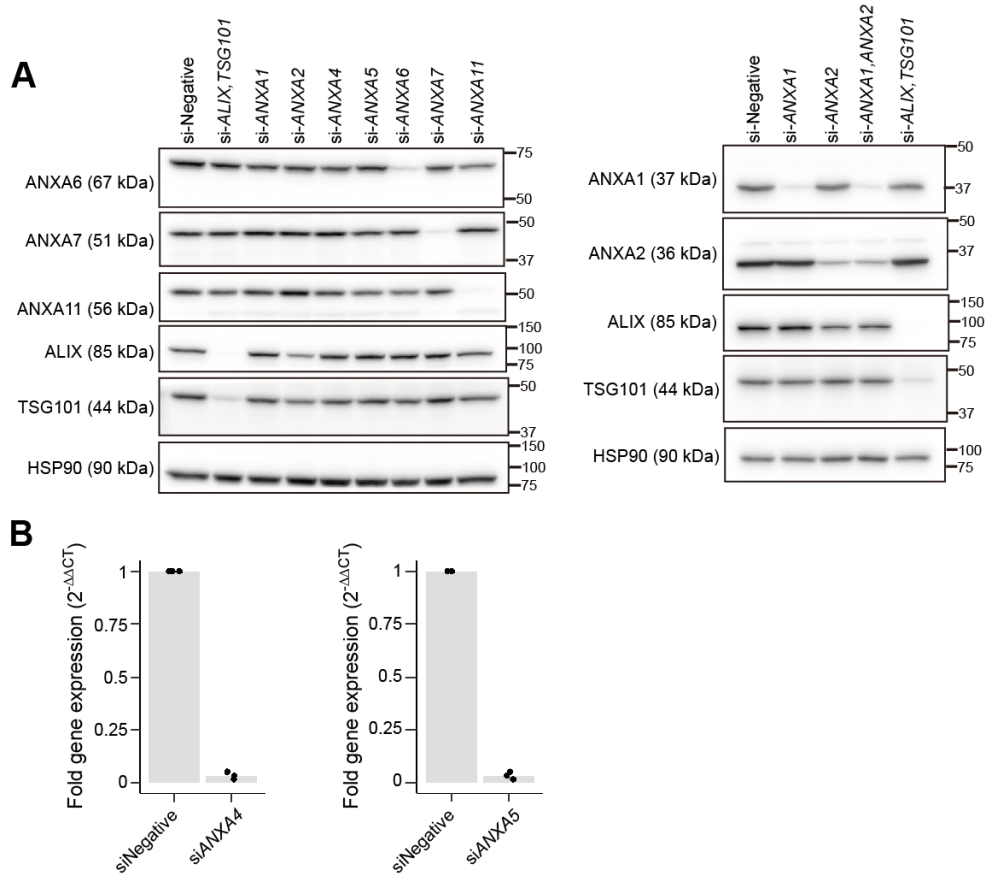


**Figure 6. siRNA-mediated gene silencing efficiency.**

(A) U2OS cells were transfected with the indicated siRNAs 72 h before collection of cell lysates. The cell lysates were then immunoblotted with the indicated antibodies to demonstrate gene silencing efficiency. (B) U2OS cells were treated with siRNA targeting *ANXA4* (left) or *ANXA5* (right) 72 h before collection of total RNA. These samples were then subjected to real-time quantitative PCR to determine gene silencing efficiency. Results are presented as  $2^{-\Delta\Delta CT}$ , calculated from the threshold cycles (CT) of the indicated siRNAs.  $\Delta\Delta CT$  values were calculated by subtracting the  $\Delta CT$  value of siNegative from the  $\Delta CT$  value of siNegative or the  $\Delta CT$  value of siANXA4/5.  $\Delta CT$  values were calculated by subtracting the CT value of the loading control GAPDH from the CT value of siNegative or siANXA4/5.  $n =$  three independent experiments.

***ANXA1, ANXA2, and ESCRTs are recruited independently.***

Next, I examined ANXA1 and ANXA2 localization during lysosome damage more closely. Since ANXA1-ANXA2 double depletion did not further delay Magic Red recovery (Figure 5), they are possibly involved in the same lysosome repair mechanism and may have similar recruitment dynamics during lysosome repair as that during plasma membrane repair [47]. Live-cell imaging of ANXA1-GFP and ANXA2-mRuby3 confirmed that ANXA1 and ANXA2 puncta formation occurred almost simultaneously at similar positions (Figure 7), suggesting that ANXA1 and ANXA2 localize to lysosomes with similar timings, possibly responding to the same signal.

I then determined whether the recruitment of ANXA1 and ANXA2 are inter-dependent by observing their localization in cells depleted of the other. After 5 min of LLOMe treatment, ANXA1 and ANXA2 could be observed on LAMP1-positive structures, representing lysosomes, in cells depleted of the other (Figure 8), indicating that they are recruited independently to damaged lysosomes.

As ANXA7 was found to recruit ESCRTs to plasma membrane injuries [50], I hypothesized that its family members ANXA1 and ANXA2 might play a similar role during lysosome repair. To test this hypothesis, I carried out immunostaining for ALIX (an ESCRT-III recruiter) and CHMP4B (an ESCRT-III component) in cells depleted of ANXA1 or ANXA2. ALIX and CHMP4B recruitment to damaged lysosomes was suppressed in ALIX-TSG101-depleted cells but unaffected in cells depleted of ANXA1, ANXA2, or both (Figure 9). Moreover, ESCRT recruitment to damaged lysosomes was not affected by depletion of the remaining annexins, ANXA4, A5, A6, A7, and A11 (Figure 10), or depletion of ALG2/PDCD6 (Figure 11), which is essential for ESCRT recruitment during plasma membrane repair [50, 52] (Figure 2). These data indicate that lysosomal ESCRT recruitment is achieved by a mechanism different from that during plasma membrane repair [50, 52] and

that the lysosome repair mechanism conducted by ANXA1 and ANXA2 is independent of ESCRTs.

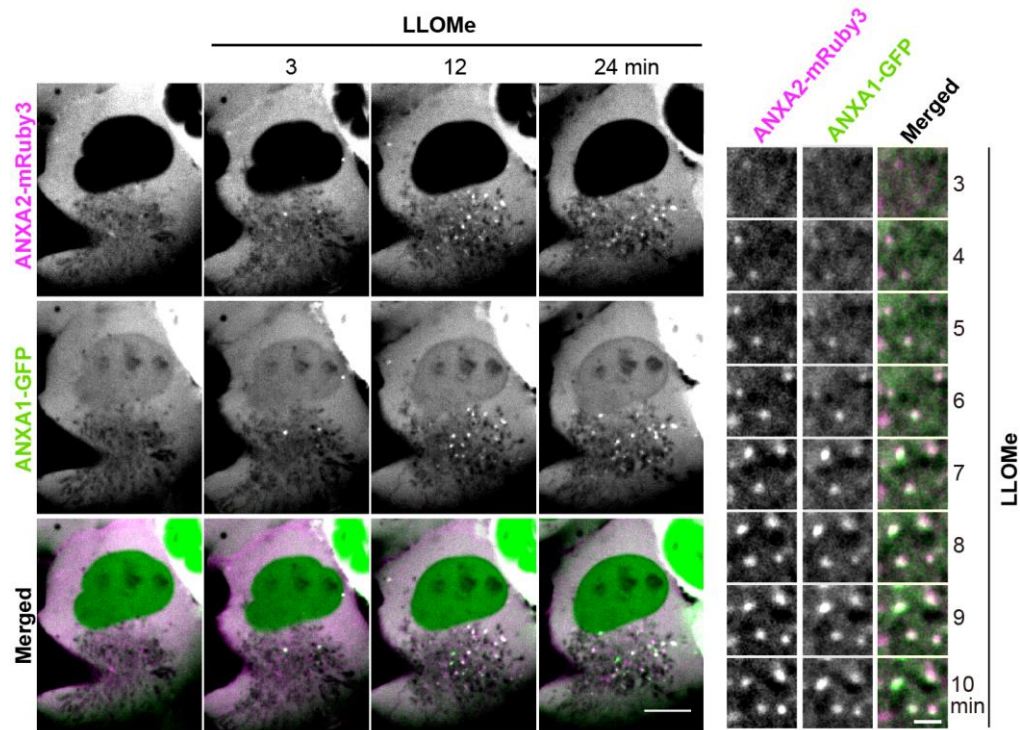


**Figure 7. ANXA1 and ANXA2 are recruited with similar dynamics.**

Time-lapse images of a U2OS cell transiently expressing ANXA1-mRuby3 and ANXA2-GFP before and during incubation with 0.3 mM LLome. Scale bar = 10 μm (main montage), 2 μm (magnified montage).



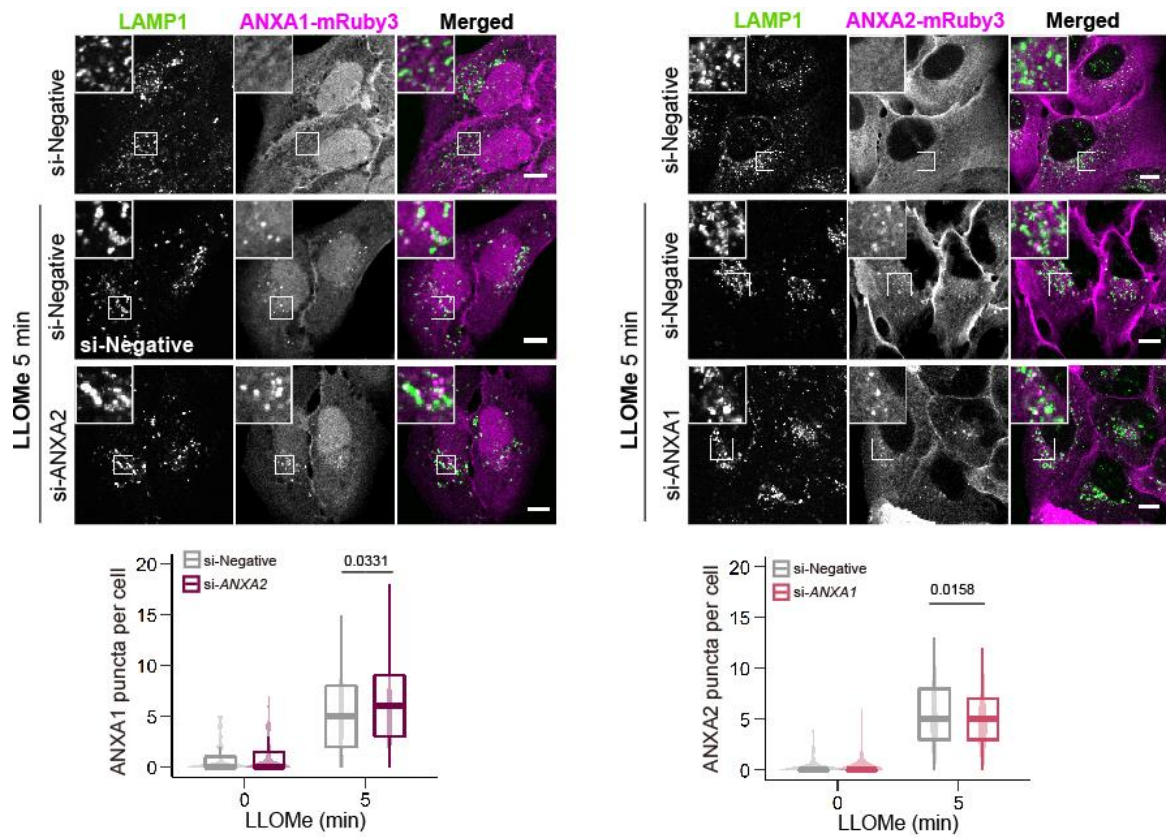


**Figure 8. ANXA1 recruitment and ANXA2 recruitment are independent of each other.**

U2OS cells stably expressing ANXA1-mRuby3 or ANXA2-mRuby3 were transfected with the indicated siRNAs 72 h before LLOMe treatment. After 5 min of incubation with 1 mM LLOMe or not, the cells were fixed and stained with anti-LAMP1 antibody. The number of ANXA1-mRuby3 or ANXA2-mRuby3 puncta were quantified for each cell. Data are presented as box plots, where the box spans the interquartile range (IQR) and the whiskers marking the within 1.5 IQR of the upper and lower quartiles. Indicated *p* values are from comparisons performed with a two-way ANOVA with Dunnett's test. *n* = 276–343 cells per group from 2 independent experiments. Scale bar = 10  $\mu$ m.



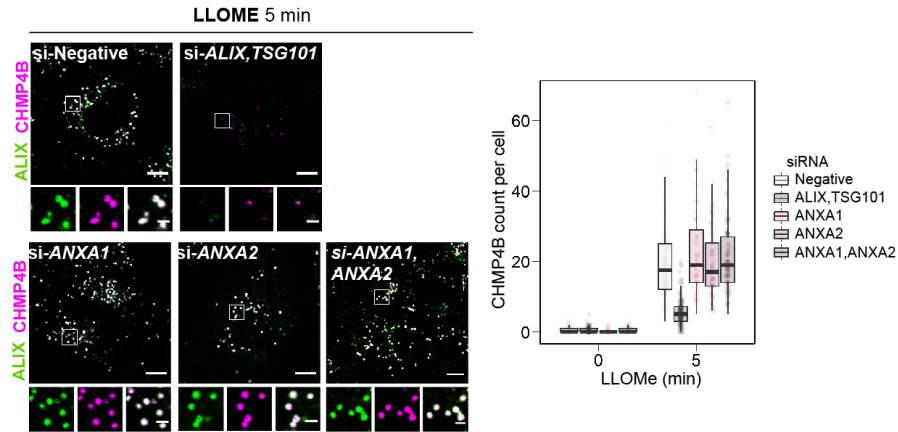


**Figure 9. Depletion of ANXA1 and/or ANXA2 did not affect ESCRT recruitment to damaged lysosomes.** U2OS cells were transfected with the indicated siRNAs 72 h before LLOMe treatment. After 5 min of incubation with 1 mM LLOMe or not, the cells were fixed and stained with antibodies targeting ALIX and CHMP4B. The number of puncta of CHMP4B, which is recruited downstream of ALIX, was counted for each cell and presented as box plots, where the box spans the interquartile range (IQR) and the whiskers marking the within 1.5 IQR of the upper and lower quartiles.  $n = 83\text{--}303$  cells from 2 independent experiments. Scale bar = 10  $\mu\text{m}$  (main), 2  $\mu\text{m}$  (inset).

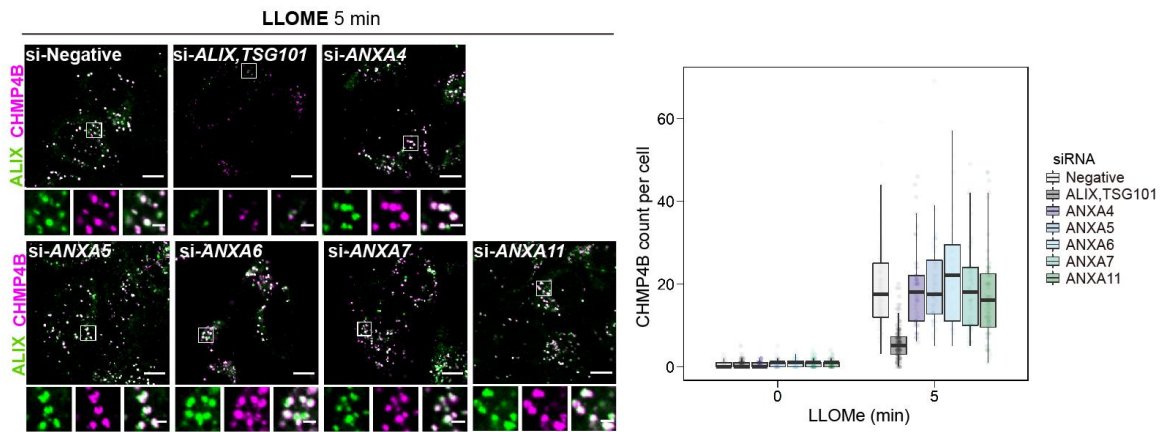


**Figure 10. Depletion of ANXA4, A5, A6, A7, or A11 did not affect ESCRT recruitment to damaged lysosomes.**

U2OS cells were transfected with the indicated siRNAs 72 h before LLOMe treatment. After 5 min of incubation with 1 mM LLOMe or not, the cells were fixed and stained with antibodies targeting ALIX and CHMP4B. The number of puncta of CHMP4B, which is recruited downstream of ALIX, was counted for each cell and presented as box plots, where the box spans the interquartile range (IQR) and the whiskers marking the within 1.5 IQR of the upper and lower quartiles.  $n = 77\text{--}309$  cells from 2 independent experiments. Scale bar = 10  $\mu\text{m}$  (main), 2  $\mu\text{m}$  (inset).

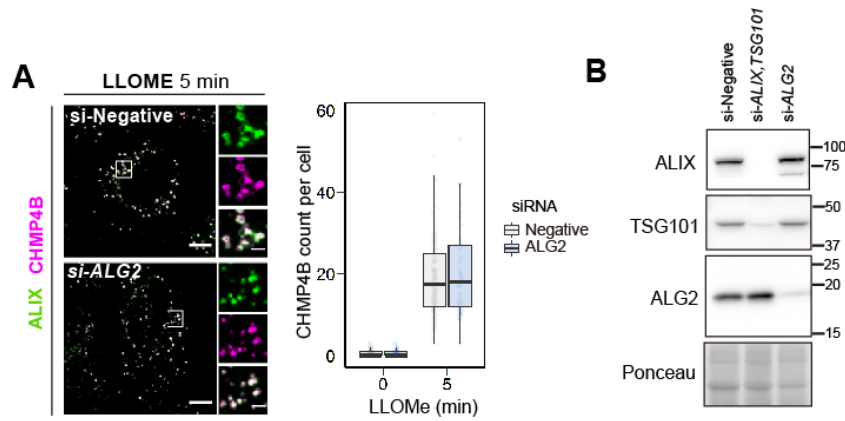


**Figure 11. Depletion of ALG2 did not affect ESCRT recruitment to damaged lysosomes.**

**(A)** U2OS cells were transfected with the indicated siRNAs 72 h before LLOMe treatment. After 5 min of incubation with 1 mM LLOMe or not, the cells were fixed and stained with antibodies targeting ALIX and CHMP4B. The number of puncta of CHMP4B, which is recruited downstream of ALIX, was counted per cell and values are presented as box plots, where the box spans the interquartile range (IQR) and the whiskers marking the within 1.5 IQR of the upper and lower quartiles.  $n = 44$  cells from 2 independent experiments. Scale bar = 10  $\mu\text{m}$  (main), 2  $\mu\text{m}$  (inset).

**(B)** U2OS cells were transfected with the indicated siRNAs 72 h before collection of cell lysates. The cell lysates were then immunoblotted with the indicated antibodies to demonstrate siRNA efficiency.

***ANXA1 and ANXA2 are recruited to a subset of damaged lysosomes in a calcium-dependent manner***

Why would there be a need for a repair mechanism by ANXA1 and ANXA2 in addition to ESCRTs? When quantifying ANXA1, ANXA2 and ESCRT puncta count in previous experiments, I noticed that the number of ANXA1 and ANXA2 puncta formed after 5 min incubation with LLOMe was ~25% that of ESCRT puncta (Figures 8-11), suggesting that the lysosomal recruitment of ANXA1 and ANXA2 might be more selective than that of ESCRTs.

I then examined the recruitment dynamics of ANXA1 tagged with mRuby3, a variant of red fluorescent protein (RFP), and the ESCRT CHMP4A tagged with HaloTag. In this experiment, FITC-conjugated 40-kDa dextran (40K-dextran) was used as an indicator of lysosome damage instead of Magic Red. In the acidic lumen of lysosomes, FITC fluorescence is quenched. Lysosome damage will result in loss of lysosomal acidification and thus brighter lysosomal FITC signal (Figure 12A). Being conjugated to the larger 40K-dextran (hydrodynamic radius = 6.6 nm; Sigma) which was reported to be mostly retained in damaged lysosomes [25], would allow constant visualization of lysosomes unlike Magic Red, which dissipates from damaged lysosomes (Figure 12A).

With live-cell imaging, I observed that ANXA1 and CHMP4A signal appeared on damaged lysosomes, as seen from their increased FITC fluorescence, with similar recruitment timings (Figure 12B). However, as LLOMe incubation progressed, more lysosomes acquired CHMP4A signal than ANXA1 signal. Many CHMP4A-positive lysosomes without ANXA1 could be observed eventually (Figures 12B and 12C). Therefore, unlike ESCRTs, ANXA1 appeared to respond to a subset of lysosomes. Based on the similar recruitment timings of ANXA1 and ANXA2 (Figure 7) as well as the smaller number of ANXA2 puncta observed

compared to that of CHMP4B (Figures 8-11), ANXA2 should also be recruited to a subset of lysosomes like ANXA1.

The reason for the discrepancy between ANXA1 (and possibly ANXA2) and ESCRT recruitment could be due to a difference in recruitment signal. Since calcium was shown to be the initial signal of lysosomal damage [21,51], the localization of ANXA1-mRuby3 and HaloTag-CHMP4A were visualized again by live-cell microscopy but this time in the presence of the calcium chelator BAPTA-AM. Under these conditions, LLOMe treatment did not result in ANXA1 nor CHMP4A puncta formation (Figures 12D and 12E), indicating that the recruitment of both ANXA1 and ESCRTs are calcium-dependent. Additionally, the effect of BAPTA-AM was stronger on ANXA1 localization: ANXA1 puncta formation was completely suppressed while a few CHMP4A puncta started to appear around 10 min of LLOMe treatment even in the presence of BAPTA-AM (Figures 12D and 12E). These CHMP4A puncta were most likely formed due to ESCRTs being directly recruited by interaction with galectins, which bind to the layer of glycosylation covering the inner surface of lysosomal membranes during lysosome damage and thus do not require calcium to localize to lysosomes [55]. Although galectin-mediated recruitment could account for some of the ESCRT localization, there should be an additional signal governing ANXA1's recruitment to damaged lysosomes since most, if not all, lysosomes release calcium when damaged and thus should recruit calcium-binding ANXA1.

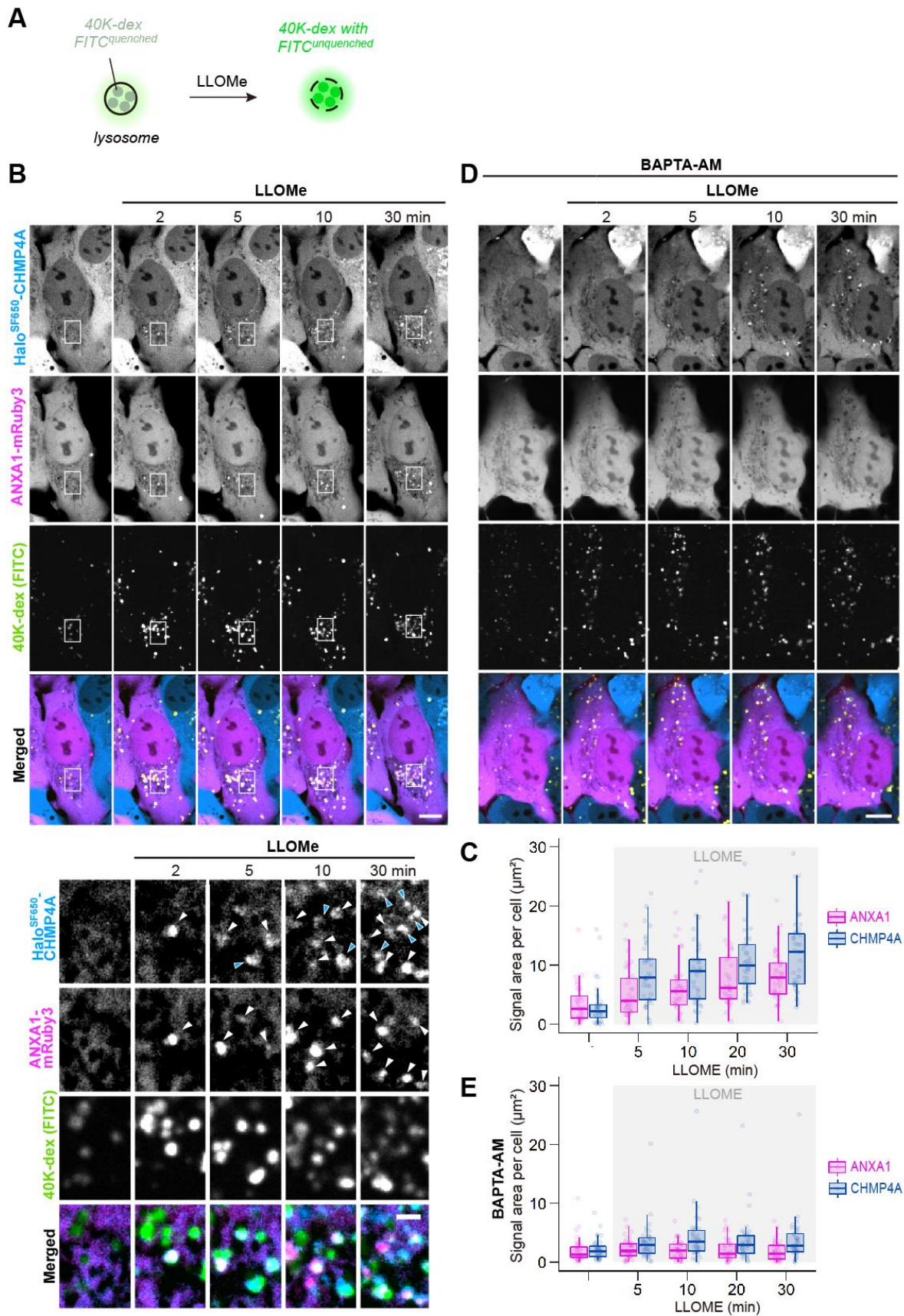


**Figure 12. ANXA1 recruitment is calcium-dependent similar to ESCRT recruitment but ANXA1 is located on fewer lysosomes.**

**(A)** FITC becomes unquenched in the higher pH of damaged lysosomes and hence can serve as an indicator of lysosome damage. 40K-dextran was previously reported to be mostly retained in LLOMe-damaged lysosomes, which allows lysosomes to be tracked even when damaged. **(B)** Time-lapse images of U2OS cells stably expressing HaloTag-CHMP4A (labeled with SaraFluor 650T (SF650) ligand) were transiently transfected with ANXA1-mRuby3 and incubated with FITC-conjugated 40K-dextran (12 h incubation, 2–4 h chase) to label lysosomes. The cells were imaged before and during incubation with 0.3 mM LLOMe. In the inset montage (below), white arrows point to puncta observed in ANXA1 and CHMP4A channels while blue arrows point to puncta observed only in the CHMP4A channel. **(C)** Quantification of ANXA1 and CHMP4A signals detected in cells treated as described in (A). Data are shown with boxplots, where the box spans the interquartile range (IQR) and the whiskers marking the within 1.5 IQR of the upper and lower quartiles.  $n = 37$  for ANXA1 and CHMP4A. **(D)** The same cells as was used in (A) but in the presence of 0.1 mM BAPTA-AM (added 1 h treatment before imaging and throughout imaging). Imaging was conducted before and during treatment with 0.3 mM LLOMe. **(E)** Quantification of ANXA1 and CHMP4A signals detected in cells treated as described in (D).  $n = 37$  for ANXA1 and CHMP4A. Scale bar = 10  $\mu\text{m}$  (main), scale bar = 2  $\mu\text{m}$  (inset montage).

***ANXA1 and ANXA2 preferentially localize to lysosomes with injuries larger than 10-kDa dextran.***

ANXA1 has eight sites for eight calcium ions [63] and ANXA2 has seven [64, 65]. In both ANXA1 [66] and ANXA2 [67], the calcium-binding sites were found to vary in binding affinity. Furthermore, *in vitro* studies with purified ANXA1 [68] and ANXA2 [68, 69] showed that the strength of their membrane association increased with calcium concentration, with one study proposing that stable membrane association would require at least seven calcium ions [69]. These findings indicate that ANXA1 and ANXA2 stably bind to membranes only when in an environment with a sufficiently high calcium concentration. Hence, I hypothesized that the additional factor governing ANXA1 and ANXA2 localization to damaged lysosomes might be related to calcium concentration and, by extension, membrane wound size. A recruitment dependency on membrane wound size has never been shown for the annexins because their membrane repair functions have been studied in the context of plasma membrane repair, where the membrane wounds are typically micrometers in size. However, lysosomes are typically 200–500 nm in diameter [70], which places the size of reparable membrane wounds in the nanometer range. Considering that the ionic radius of a calcium ion ( $\text{Ca}^{2+}$ ) is around 0.1 nm, the size of lysosomal membrane wounds would determine the amount of calcium ions released into the cytosol and in turn perhaps whether ANXA1 and ANXA2 would be recruited.

To test my hypothesis that ANXA1 and ANXA2 are recruited to lysosomes with larger injuries, I carried out live-cell imaging of ANXA1-GFP and HaloTag-CHMP4A with lysosomes preloaded with tetramethylrhodamine (TMR)-conjugated 10-kDa dextran serving as the lysosomal wound size marker. Incubation with LLOMe resulted in the gradual reduction of 10K-dextran<sup>TMR</sup> signal from lysosomes, with the rate of loss varying among lysosomes (Figure 13), indicating the effect of LLOMe is not uniform across lysosomes as

previously reported [25]. The heterogeneity of lysosome damage is most likely due to acidity and enzymatic activity among lysosomes being heterogenous, resulting in different amounts of membranolytic LLOMe polymers in each lysosome [61, 71, 72]. This trait of lysosomes allowed me to observe the differential recruitment of ANXA1 and CHMP4A: ANXA1 was found on a lysosome that had rapidly lost 10K-dextran<sup>TMR</sup> but not on the neighboring lysosomes that were releasing 10K-dextran<sup>TMR</sup> at a slower rate (Figure 13, magnified montage). The ANXA1-positive lysosome must have had membrane wounds considerably larger than 10K-dextran<sup>TMR</sup> to allow their rapid release into the cytosol. By contrast, its neighboring lysosomes had smaller membrane wounds that allowed only gradual leakage of 10K-dextran<sup>TMR</sup>. CHMP4A also appeared on the more heavily damaged lysosome at the same time as ANXA1. However, ESCRTs may be more sensitive to the damage signal, since CHMP4A gradually accumulated on the neighboring lysosomes with less severe injuries that never acquired ANXA1 signal (Figure 13, magnified montage). Therefore, ANXA1 may be preferentially recruited to lysosomes with injuries exceeding the size of 10K-dextran<sup>TMR</sup>.

To confirm whether ANXA1 and ANXA2 are preferentially recruited to more heavily damaged lysosomes, I proceeded to quantify their presence in lysosomes with Alexa Fluor 647 (A647)-conjugated 10K-dextran (10K-positive) and in lysosomes without 10K-dextran<sup>A647</sup> (10K-negative) after exposure to LLOMe. Lysosomes were marked with TMEM192-GFP [73] and classified as 10K-positive or 10K-negative based on whether their 10K-dextran fluorescence intensity exceeded a threshold determined from 10K-dextran intensity before LLOMe incubation (Figure 14A). Classification of lysosomes as 10K-positive or 10K-negative was conducted for cells at the 16 min mark of LLOMe incubation, which was the last time point when most cells still had strongly 10K dextran<sup>A647</sup>-positive lysosomes. After classifying lysosomes based on 10K-dextran<sup>A647</sup> intensity, they were further categorized as positive or negative for ANXA1, ANXA2, or CHMP4A (Figure 14A).



CHMP4A was present on ~96% of 10K-negative lysosomes (Figure 14B), indicating that most of the lysosomes in this category required repair. By contrast, it was found on ~61% of 10K-positive lysosomes (Figure 14B), making CHMP4A ~1.6 times more likely to be found on 10K-negative lysosomes. This preference could be attributed to the higher likelihood of 10K-negative lysosomes requiring repair; in other words, the ~39% of 10K-positive lysosomes without CHMP4A could be lysosomes that did not require repair as they were either entirely undamaged or had injuries too mild to recruit ESCRTs (e.g., transient membrane pores). However, ANXA1 and ANXA2 showed a considerably stronger preference for 10K-negative lysosomes: they were ~7-8 times more likely to be present on lysosomes in this category (Figure 14B). Even if I were to assume that 39% of the 10K-positive lysosomes were undamaged (based on the CHMP4A data) and exclude them from the comparison, ANXA1 and ANXA2 would still be ~4-4.5 times more likely to be present on 10K-negative lysosomes. Hence, ANXA1 and ANXA2 are preferentially recruited to lysosomes with injuries larger than 10K-dextran.

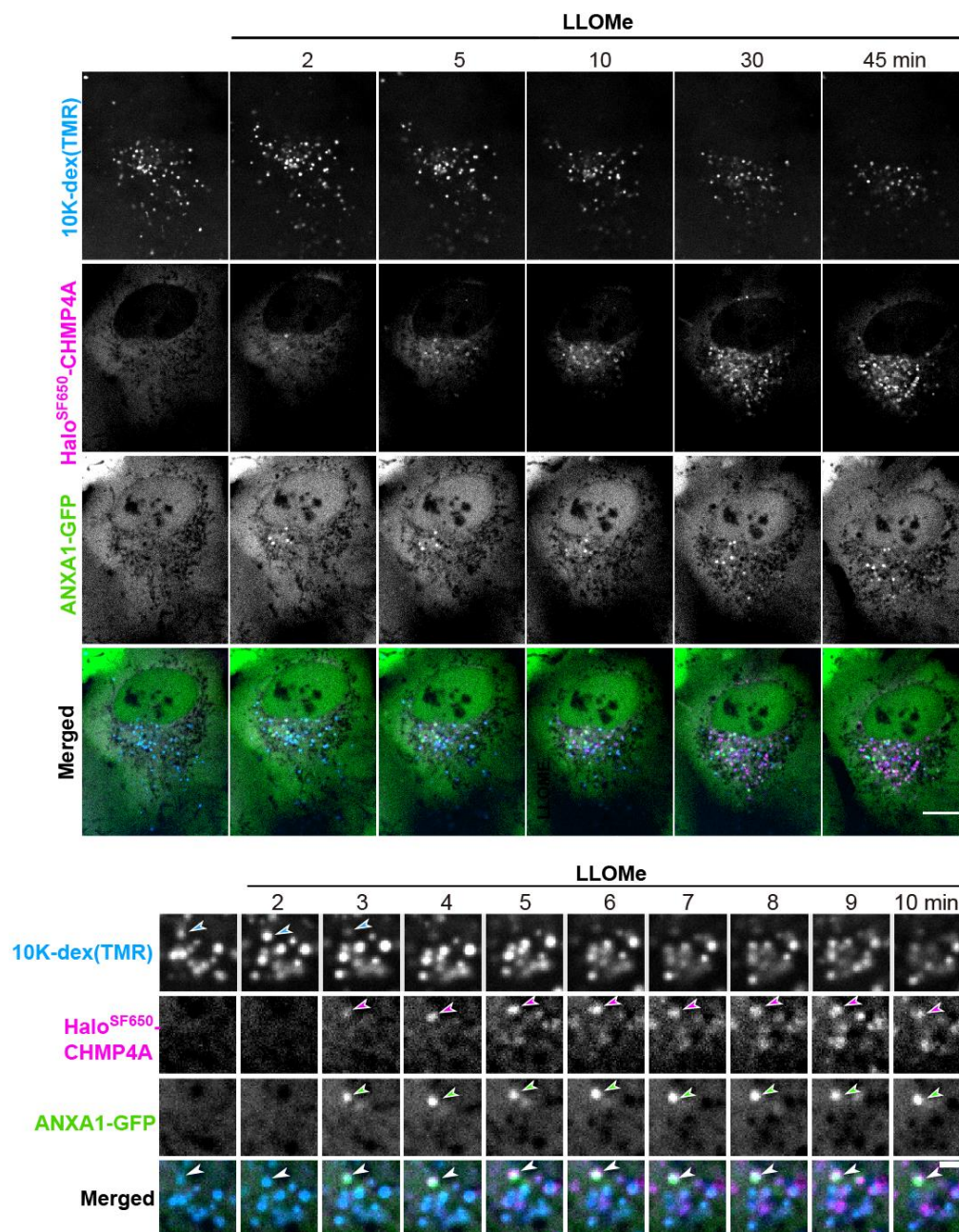


**Figure 13. ANXA1 localizes to lysosomes that rapidly lose 10K-dextran.**

Time-lapse images of a U2OS cell stably expressing HaloTag-CHMP4A (labeled with SaraFluor 650T (SF650)-conjugated ligand) and transiently expressing ANXA1-mRuby3 and ANXA2-GFP before and during incubation with 0.3 mM LLOMe. The lysosomes were labeled with Alexa 647-conjugated 10K-dextran (12 h incubation, 2–4 h chase). Arrows point to the lysosome that acquired ANXA1 signal. Scale bar = 10  $\mu$ m (above); 2  $\mu$ m (below).

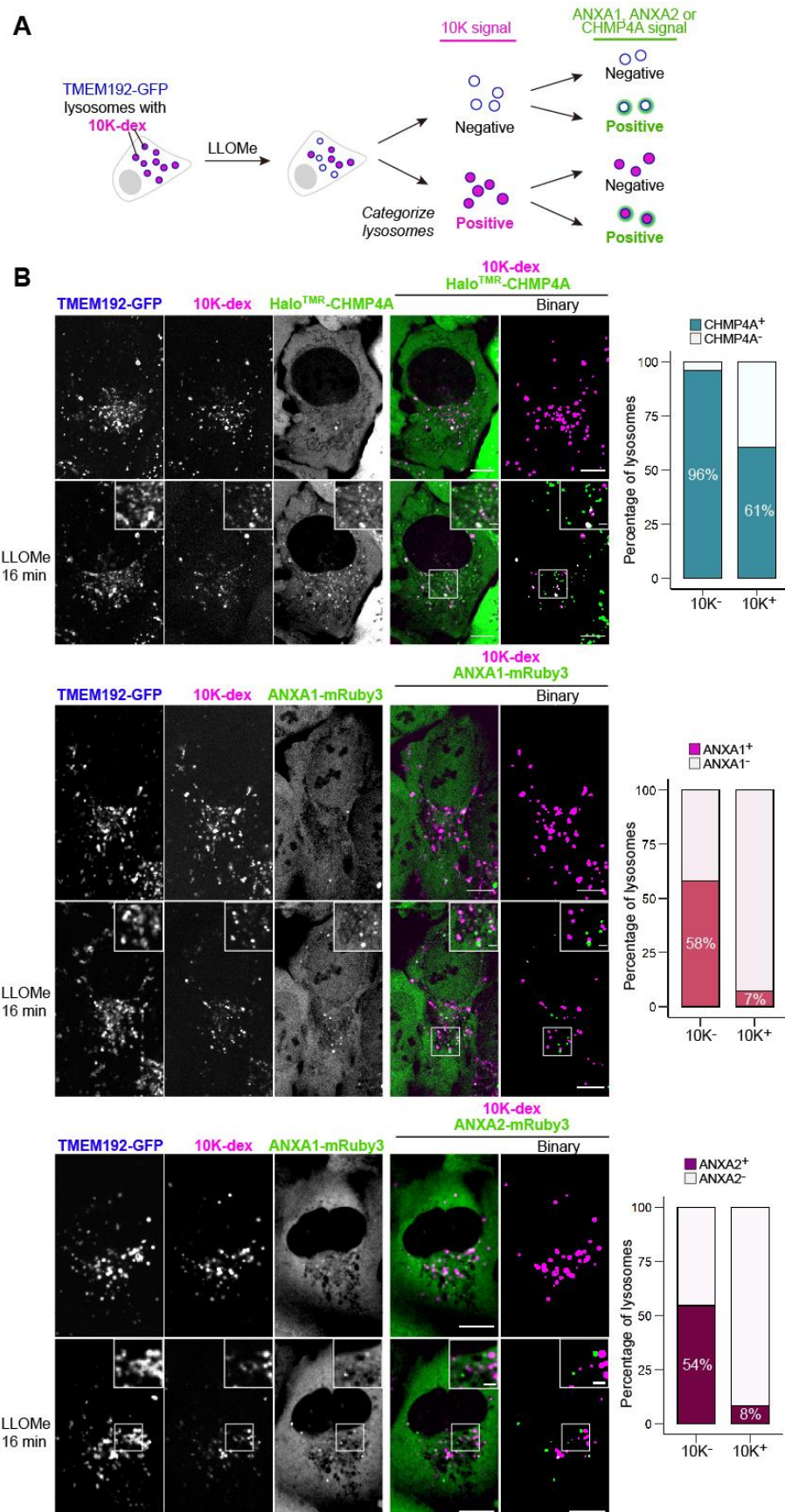


**Figure 14. ANXA1 preferentially localizes to lysosomes without 10K-dextran.**

**(A)** Schematic of the experiment. U2OS cells stably expressing TMEM192-GFP and ANXA1-mRuby3, ANXA2-mRuby3, or Halo<sup>TMR</sup>-CHMP4A (HaloTag-CHMP4A labeled with tetramethylrhodamine (TMR)-conjugated ligand). Their lysosomes were loaded with Alexa Fluor 647 (A647)-conjugated 10K-dextran (12 h incubation, 2–4 h chase) before being incubated with 1 mM LLOMe. To obtain the distribution of ANXA1, ANXA2, and the ESCRT CHMP4A among LLOMe-exposed lysosomes that still retained 10K-dextran<sup>A647</sup> (10K-positive) or lost 10K-dextran<sup>A647</sup> (10K-negative), TMEM192-GFP marked regions of interest were first obtained. Since TMEM192 is a lysosomal membrane protein, these regions of interest represent lysosomes. These regions of interest were then classified as 10K-positive or 10K-negative with a threshold based on the dextran signals before LLOMe incubation. Finally, they were further classified into lysosomes with or without ANXA1, ANXA2, or CHMP4A. **(B)** The distribution of CHMP4A, ANXA1, and ANXA2 among 10K-positive and 10K-negative lysosomes at the 16 min time point of 1 mM LLOMe incubation (when most cells still had 10K dextran-positive lysosomes). *n* = 1858 lysosomes for ANXA1-mRuby3; 592 lysosomes for ANXA2-mRuby3; 2086 lysosomes for Halo-CHMP4A from >40 cells. Scale bar = 10  $\mu$ m; 2  $\mu$ m (inset).

### ***ANXA1 and ANXA2 may promote repair of larger injuries***

Next, I determined whether more heavily damaged lysosomes that recruited ANXA1 (and likely ANXA2 as well) could have their activity restored. I measured the intensity profiles of FITC-conjugated 40K-dextran (hydrodynamic radius = 6.6 nm; Sigma) of individual lysosomes in addition to the intensity profiles of ANXA1-mRuby3 and HaloTag-CHMP4A, which are not released from lysosomes transiently permeabilized by brief LLOMe exposure [25]. Lysosome damage would result in unquenching of FITC fluorescence due to increased luminal pH and FITC fluorescence would be quenched again after lysosome repair (Figure 15A). These lysosomes could be separated into two categories, ANXA1-positive and ANXA1-negative. Lysosomes in the former category presumably had larger injuries while those in the latter category were more mildly damaged. Both categories of lysosomes showed re-quenching of FITC signal during the washout following 1.5 min of LLOMe exposure (Figure 15B), showing that both categories of lysosomes could be repaired. Moreover, ANXA1-positive lysosomes appeared to re-acidify slightly faster (Figure 15B), despite them being more likely to be heavily damaged. This suggests that lysosomes with larger injuries can also be efficiently repaired. Additionally, the FITC fluorescence intensity profiles of lysosomes with only ANXA1 signal were obtained from cells depleted of ALIX and TSG101. After 1.5 min of exposure to LLOMe, the FITC fluorescence levels of lysosomes with only ANXA1 also returned to pre-damage levels (Figure 15C), suggesting that ANXA1-mediated repair alone can resolve lysosome damage.

Since ANXA1 and ANXA2 are preferentially recruited to damaged lysosomes with larger injuries allowing the passage of 10K-dextran (Figures 13 and 14), their primary role during lysosome repair might be to ensure efficient repair of lysosomal membrane wounds exceeding 4.6 nm (the diameter of 10K-dextran). The larger the membrane wound, the greater the possibility of lysosomal contents leaking into the cytosol. Hence, ANXA1- and

ANXA2-mediated lysosome repair might be particularly important in preventing excessive lysosomal leakage. To test this hypothesis, I examined the rate of A647-conjugated 10K-dextran release from lysosomes in cells depleted of ANXA1, ANXA2, or ALIX-TSG101 during the washout following 1.5 min exposure to LLOMe. Inefficient or lack of repair was expected to result in increased rate of 10K-dextran<sup>A647</sup> loss (Figure 16A).

After being exposed to 1.5 min of LLOMe, 10K-dextran fluorescence intensity increased briefly from being unquenched in damaged lysosomes (Figure 16B). In cells treated with negative control siRNA, the intensity returned to levels comparable to that in untreated cells within 20 min, which corresponds with the time taken for Magic Red recovery (Figure 5B vs. Figure 16B). The lack of further dextran<sup>A647</sup> loss indicates that lysosomes were repaired without detectable loss of 10K-dextran<sup>A647</sup>, which agrees with a previous report on the retention of molecules larger than 10 kDa in LLOMe-treated lysosomes [62]. In ALIX-TSG101 depleted cells, 10K-dextran<sup>A647</sup> intensity continued to decrease after the 20 min time point. Although the difference between 10K-dextran<sup>A647</sup> intensity of ALIX-TSG101 depleted cells and of control cells at the end of observation (40 min of washout) was not found to be statistically significant, the downward trend of ALIX-TSG101 depleted cells' 10K-dextran<sup>A647</sup> loss suggest that ESCRTs also contribute to preventing lysosomal leakage.

In contrast to negative control cells and ALIX-TSG101 double depleted cells, ANXA1-depleted and ANXA2-depleted cells showed faster and more drastic 10K-dextran<sup>A647</sup> loss, which reached ~75% of pre-LLOMe intensity levels by the end of observation (Figure 16B). The speed and degree of 10K-dextran<sup>A647</sup> loss in ANXA1- and ANXA2-depleted cells suggest that without ANXA1 and ANXA2, membrane wounds allowing rapid loss of 10K-dextran could not be quickly resolved. Hence, larger injuries may require the activity of ANXA1 and ANXA2 to be resolved efficiently, to avoid excessive loss of lysosomal contents.



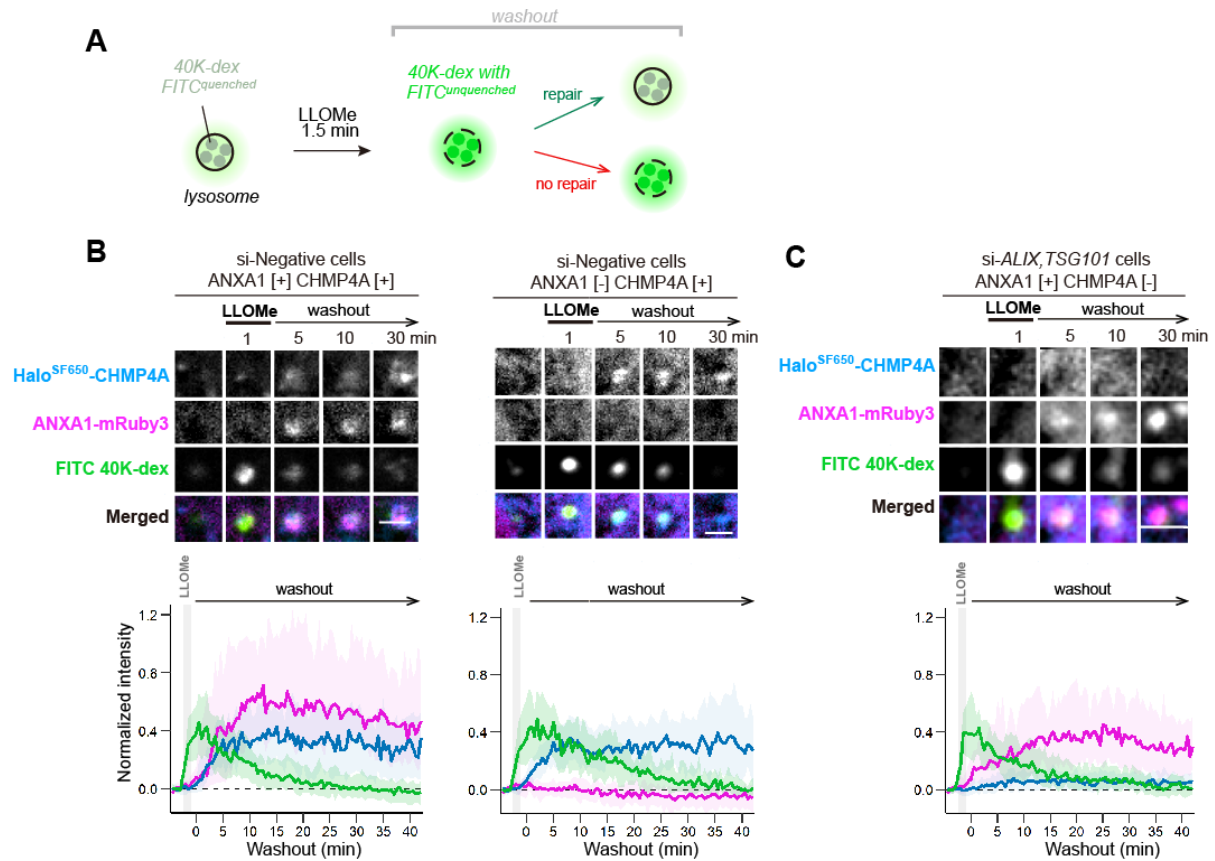


**Figure 15. ANXA1-positive damaged lysosomes can recover acidity even without ESCRT.**

(A) FITC-conjugated 40K-dextran intensity levels were measured for individual lysosomes obtained from cells exposed to 1.5 min of 0.3 mM LLOMe. (B) FITC-conjugated 40K-dextran intensity levels of ANXA1[+]CHMP4A[+] lysosomes and ANXA1[-]CHMP4A[+] from cells transfected with negative control siRNA. In the plots, lines trace median values and ribbons mark the 25<sup>th</sup> and 75<sup>th</sup> percentile values. (C) FITC-conjugated 40K-dextran intensity levels of ANXA1[+]CHMP4A[-] lysosomes from cells transfected with siRNA targeting the ESCRTs ALIX and TSG101. In the plot, lines trace median values and ribbons mark the 25<sup>th</sup> and 75<sup>th</sup> percentile values.  $n = 52$  for ANXA1[+]CHMP4A[+], 51 for ANXA1[-]CHMP4A[+] lysosomes, 27 for ANXA1[+]CHMP4A[-] from >10 cells. Scale bar = 2  $\mu$ m.

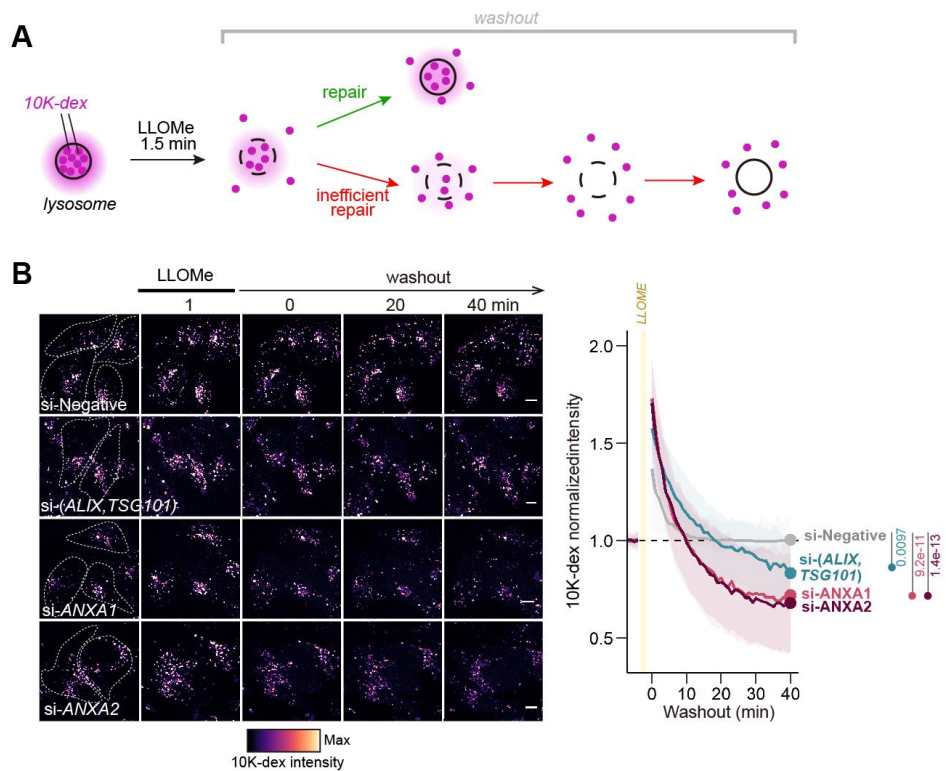


**Figure 16. 10K-dextran release is exacerbated by depletion of ANXA1 or ANXA2.**

(A) After exposure to LLOMe, lysosomes with larger injuries will release 10K-dextran. If repaired, 10K-dextran release would be stemmed. If not repaired efficiently, 10K-dextran would continue to leak out of lysosomes. (B) U2OS cells transfected with the indicated siRNAs for 72 h before imaging were labeled with Alexa 647-conjugated 10K-dextran (12 h incubation, 2 h chase). The fluorescence intensity of dextran<sup>A647</sup> was measured per cell with a threshold determined automatically from the fluorescence intensity of four timepoints before a 1.5 min exposure to 0.3 mM LLOMe. In the plot, lines trace median values and ribbons mark the 25<sup>th</sup> and 75<sup>th</sup> percentile values. The mean value of the last timepoint (40 min washout) for each siRNA was compared with the mean of the negative control using a two-way ANOVA with Dunnett's test.  $p$  values as indicated. Scale bar = 10  $\mu$ m.  $n$  = 164-377 cells from 3 independent experiments.



## Discussion

The importance of annexins to plasma membrane repair is well established [28-30] but whether they can repair other organellar membranes has not been investigated. In this study, I have shown that although all ubiquitously expressed annexins (A1, A2, A4, A5, A6, A7, and A11) localize to damaged lysosomes, only ANXA1 and ANXA2 are important for efficient lysosome repair. This finding expands on previous observations of ANXA2 localization to lysosomes containing membrane-destabilizing wear debris [54]. Recruitment of ANXA1 and ANXA2 to damaged lysosomes is calcium-dependent and shows a strong preference for lysosomes with membrane injuries larger than 4.6 nm in diameter, possibly the larger amount of calcium being released from such lysosomes. After localization, they likely act to suppress lysosomal leakage and promote lysosome repair independently of ESCRTs. ANXA1 and ANXA2-mediated lysosome repair is thus an additional means of maintaining lysosomal integrity.

### *ANXA1 and ANXA2 as an additional lysosome repair mechanism*

The finding that ESCRT-mediated repair may not be sufficient for sealing membrane wounds exceeding 4.6 nm—the diameter of 10K-dextran—was unexpected at first. It is widely accepted that ESCRT-mediated membrane fission during intraluminal vesicle formation is highly efficient [33, 34, 37] but this might not directly apply to membrane wound-resealing, which is a process different from membrane fission since the former occurs on an intact membrane while the latter occurs on a perforated membrane (Figure 3A and B). If the widely accepted model is true—that ESCRTs induce membrane budding and subsequent excision of the wound-containing membrane area (Figure 3B)—then it would be reasonable to posit that longer ESCRT spirals would be required to repair larger wounds,

leading to lower ESCRT-mediated repair efficiency. ANXA1 and ANXA2-mediated repair would then be employed to increase chances of lysosome repair and prevent its elimination by lysophagy (Figures 17A and 17B). ESCRTs and ANXA1/A2 may carry out separate mechanisms but both are working towards the same goal of restoring lysosomal membrane integrity (Figures 17A and 17B), as they do during plasma membrane repair [28-30] (Figure 2). The ESCRT-mediated repair mechanism itself and its effectiveness with regards to membrane pore resealing would have to be further investigated. Nevertheless, maintaining the integrity of the plasma membrane and lysosomal membrane are essential for cell survival so having multiple mechanisms to do so would only be advantageous to the cell.

#### ***How do ANXA1 and ANXA2 repair membrane injuries?***

Although they were not found to be required for lysosome repair, it remains possible that the other widely expressed annexins (ANXA4, A5, A6, A7, and A11) contribute to lysosome repair alongside ANXA1 and ANXA2, based on their plasma membrane repairing activities [28-30]. They could be functionally redundant and therefore produce no observable phenotype when depleted individually. Conversely, it is also possible that only ANXA1 and ANXA2 are functionally involved in ANX-mediated lysosome repair. ANXA1 and ANXA2 are most similar to each other within the ANX family and even induce similar membrane deformations *in vitro* [74]. Despite their similarities, ANXA1 and ANXA2 are not redundant since individual depletion was able to suppress lysosome repair in this study (Figures 5 and 16) and plasma membrane repair in previous studies [40, 42-44]. Hence, it is highly likely that ANXA1 and ANXA2 are separately necessary to mediate membrane wound resealing during lysosome repair and plasma membrane repair. *In vitro* experiments with purified annexins and supported lipid bilayers demonstrated that ANXA1 and ANXA2 induce membrane deformations, specifically “membrane folding and blebbing initiated from

membrane structural defects”, that were physically different from those by other annexins [74]. This method of membrane deformation might be particularly suited to resolving lysosomal membrane injuries.

Details of ANXA1- and ANXA2-mediated lysosome repair are still unclear. Based on the findings on ANXA1- and ANXA2-mediated plasma membrane repair [47, 75] and those from *in vitro* ANXA1 and ANXA2 studies [74, 76-81], I speculate that ANXA1 and ANXA2 might form a ‘cap’ over the membrane wound, which helps to prevent further leakage of lysosomal contents. ANX cap formation (consisting of ANXA1, A2, A5, and A6) at injury sites was previously reported for damaged plasma membrane of zebrafish [75] and human cells [47, 49]. Subsequently, since the membrane-deforming activities ANXA1 and ANXA2 are well-established [74, 76-81], the ANXA1 and ANXA2 proteins amassed at the injury site could deform the membrane areas around the membrane wound, thereby promoting wound sealing (Figure 17C). *In vitro* studies and higher resolution imaging techniques would be more suitable to investigate the activities of ANXA1, ANXA2, and the other annexins toward membrane wounds of various sizes and in varying calcium concentrations.

### ***How are ESCRTs recruited to damaged lysosomes?***

In this study, I found that the mechanism underlying calcium-dependent recruitment of ESCRTs to damaged lysosomes is different from that employed for plasma membrane injuries. ESCRT recruitment to damaged lysosomes requires neither ANXA7 (or any other annexin) nor ALG2/PDCD6, which have been reported to be important for recruitment to injury sites on the plasma membrane [50, 52].

The calcium-dependent activation of LRRK2 (leucine-rich repeat kinase 2) and its phosphorylation of Rab8A was recently reported to be important for ESCRT recruitment to LLOMe-damaged lysosomes based on the finding that ESCRT recruitment was severely

reduced in cells without LRRK2 or Rab8A [53]. However, several unanswered questions remain: (1) how is LRRK2 able to respond to changing calcium levels?, (2) are Rab3A, Rab10, and Rab35, which were previously reported to be phosphorylated by LRRK2 during lysosomal stress [82], targets of LRRK2 during lysosomal damage?, and (3) how does Rab8A conduct ESCRT recruitment?. During osmolytic lysosomal stress, LRRK2 was reported to be recruited to lysosomes by Rab7L1 [82], indicating to further upstream factors. Furthermore, it is likely that LRRK2-dependent ESCRT recruitment is not the only ESCRT recruitment pathway because LRRK2 is recruited to only a subset of damaged lysosomes [53, 83]. Clarifying the mechanistic details of ESCRT recruitment to damaged lysosomes will provide insight to the sensitivity of ESCRT recruitment to mild lysosomal damage and perhaps how ESCRTs assemble around membrane wounds.

#### ***Other repair mechanisms for damaged lysosomes***

Additional lysosome repair mechanisms may exist. The exposure of sphingomyelin on the cytosolic leaflet of damaged lysosomal membranes [84, 85] and the subsequent hydrolysis of the exposed sphingomyelin to ceramide by neutral sphingomyelinase (SMPD3) [85] were recently reported. The increase in ceramide levels was found to promote membrane repair in an ESCRT-independent manner [85]. Although the exact mechanism of ceramide-based repair is unclear, a model could be built from similar findings obtained from studies on plasma membrane repair and the properties of ceramide. Ceramide has a much smaller head group and is less hydrophilic than sphingomyelin [86]. When present abundantly in a lipid bilayer, ceramides tend to assemble into negatively curved domains that then separate from the membrane as vesicles [87-89]. As ceramide domains generated by acid sphingomyelinase (SMPD1) in response to calcium influx through plasma membrane injuries have been reported to be crucial for efficient endocytosis-based plasma membrane repair [90,

91], it is possible that the assembly of ceramide domains in lipid bilayers could also result in repair in the form of vesiculation *in vivo*. These findings suggest that the generation of ceramide on damaged lysosomal membranes would repair the membrane in a similar manner. Furthermore, as ANXA1 has been reported to have higher affinity with ceramide-containing membranes [92], the increased presence of ceramide could also promote ANXA1- and ANXA2-mediated repair. This model of ceramide-based membrane repair would have to be further investigated to address questions such as whether ceramide domains are formed on damaged lysosomal membranes, whether ceramide-rich intralysosomal vesicles are formed from damaged lysosomal membranes, and whether there is a relationship between ceramide and ANXA1/A2 during lysosome repair.

***Membrane properties as a possible reason for the differences between plasma membrane repair and the lysosome repair***

As shown in this study, the mechanisms for plasma membrane repair and lysosome repair do not overlap completely. Although both employ ESCRTs and annexins, the mechanistic details vary, such as the importance of nearly all ubiquitously expressed annexins in plasma membrane repair in contrast to only ANXA1 and ANXA2 for lysosome repair. Besides the extent of damage, another major factor dictating the type of repair mechanism could be the membrane properties of the plasma membrane and the lysosomal membrane because pore sealing requires membrane tension to be reduced and pore edge tension to be increased [93]. These modifications that end in membrane repair are facilitated by membrane repair proteins. The efficiency of repair would thus depend on how suited the membrane repair mechanism is to the properties of the damaged membrane.

Since they differ in lipid composition, density of membrane proteins, and presence of external attachments [93], the plasma membrane and the lysosomal membrane should have

different membrane properties. Indeed, studies with lipid packing probes have showed that lysosomal membranes are less ordered, more loosely packed [94, 95], and lower in tension [96] than the plasma membrane. In line with these findings are reports of lysosomal membranes having lower levels of the order-promoting lipid cholesterol [94, 97] and smaller numbers of proteins than the plasma membrane ( $\sim 700$  particles per  $\mu\text{m}^2$  for isolated mouse liver lysosomes [98] vs.  $\sim 4,500$  particles per  $\mu\text{m}^2$  for plasma membranes of rat cardiac cells [99], obtained by freeze-fracture electron microscopy). Furthermore, unlike the plasma membrane which is mostly anchored to the actin cortex (a network of actin filaments and actin-binding proteins) [100], lysosomal membranes are mostly free of external attachments as they are highly dynamic organelles that move freely on microtubules around the cell to fuse or make contact with other organelles [101]. Taken together, these findings suggest that lysosomal membranes are more malleable than the plasma membrane and that lysosomal membrane injuries can be more easily resolved. Furthermore, unlike lysosomes which can be cleared by autophagy when damaged beyond repair, repair is the only way to resolve plasma membrane damage. Hence, resolving plasma membrane injuries might require a set of stronger repair mechanisms that can efficiently remodel the more unyielding plasma membrane, including its underlying actin cortex, to resolve membrane injuries regardless of size.

## ***Conclusion***

Being sites of degradation, recycling, and metabolic signaling, maintaining the integrity of lysosomes is integral to cellular homeostasis. Therefore, it is reasonable for the cell to have more than one mechanism to repair lysosomes and that the mechanisms would be shared with plasma membrane repair. Although this study has identified an additional lysosome repair mechanism in ANXA1 and ANXA2, many details remain unclear,

particularly the exact mechanisms of membrane wound resolution by ANXA1, ANXA2 and by ESCRTs. Clarifying such mechanisms will contribute to our understanding on cell biology and possibly to the design of less disruptive endocytosis-based drug delivery systems [102] as well as more effective cytotoxic therapeutics against cancer cells [103, 104].

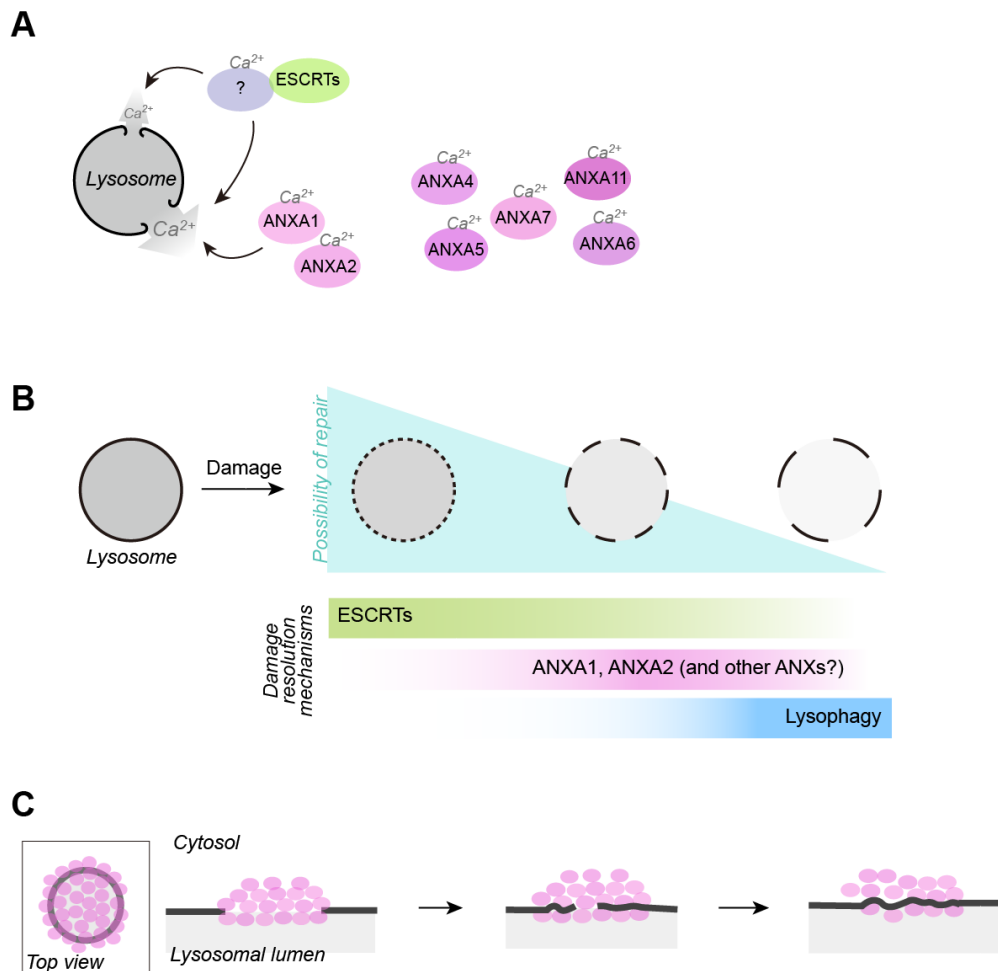


**Figure 17. ANXA1 and ANXA2 may constitute an additional repair mechanism to promote repair and preservation of damaged lysosomes.**

(A) During lysosome repair, different mechanisms may be employed according to damage severity. Membrane wounds less than the size of 10K-dextran (~4.2 nm across) are resolved by ESCRTs whereas those larger recruit ANXA1, ANXA2, and most likely other annexins. Annexin preference for larger membrane wounds might be related to the higher levels of calcium released. (B) Lysosomes can be damaged by various agents, including lysosomal membrane permeabilizing drugs, aberrant protein aggregates, long-term accumulation of waste material, and phagocytosed pathogens. The amount of damage dealt by each membrane-destabilizing agent differs and is resolved accordingly, with the possibility of repair decreasing with increasing damage severity. Minor lysosomal membrane permeabilization has the highest possibility of repair by ESCRTs. When the degree of membrane destabilization increases, ANXA1 and ANXA2 (and maybe other annexins) become involved to promote repair and preservation of the damaged lysosomes. Eliminating the damaged lysosome by lysophagy is the last resort taken when the lysosome is damaged beyond repair. (C) A speculative model of how ANXA1- and ANXA2-mediated lysosome repair could be achieved. ANXA1 and ANXA2 might congregate around and over the injury site, where the calcium concentration is the highest. The binding of ANXA1 and ANXA2 to that region would then be a 'cap', preventing further lysosomal leakage, as proposed for plasma membrane repair. Furthermore, with their membrane-deforming and membrane-aggregating activities, ANXA1 and ANXA2 might also promote wound sealing by drawing the wound edges together.



## References

1. Xu, H. and D. Ren, *Lysosomal physiology*. Annu Rev Physiol, 2015. **77**: p. 57-80.
2. Ballabio, A. and J.S. Bonifacino, *Lysosomes as dynamic regulators of cell and organismal homeostasis*. Nat Rev Mol Cell Biol, 2020. **21**(2): p. 101-118.
3. Halle, A., et al., *The NALP3 inflammasome is involved in the innate immune response to amyloid-beta*. Nat Immunol, 2008. **9**(8): p. 857-65.
4. Freeman, D., et al., *Alpha-synuclein induces lysosomal rupture and cathepsin dependent reactive oxygen species following endocytosis*. PLoS One, 2013. **8**(4): p. e62143.
5. Emmerson, B.T., et al., *Reaction of MDCK cells to crystals of monosodium urate monohydrate and uric acid*. Kidney Int, 1990. **37**(1): p. 36-43.
6. Thibodeau, M.S., et al., *Silica-induced apoptosis in mouse alveolar macrophages is initiated by lysosomal enzyme activity*. Toxicol Sci, 2004. **80**(1): p. 34-48.
7. Duewell, P., et al., *NLRP3 inflammasomes are required for atherogenesis and activated by cholesterol crystals*. Nature, 2010. **464**(7293): p. 1357-1361.
8. Kirkegaard, T., et al., *Hsp70 stabilizes lysosomes and reverts Niemann-Pick disease-associated lysosomal pathology*. Nature, 2010. **463**(7280): p. 549-53.
9. Li, Y., et al., *The lysosomal membrane protein SCAV-3 maintains lysosome integrity and adult longevity*. J Cell Biol, 2016. **215**(2): p. 167-185.
10. Gupta, S., et al., *Lysosomal retargeting of Myoferlin mitigates membrane stress to enable pancreatic cancer growth*. Nat Cell Biol, 2021. **23**(3): p. 232-242.
11. Deng, D., et al., *Loss of membrane cholesterol influences lysosomal permeability to potassium ions and protons*. Biochim Biophys Acta, 2009. **1788**(2): p. 470-6.

12. Appelqvist, H., et al., *Sensitivity to lysosome-dependent cell death is directly regulated by lysosomal cholesterol content*. PLoS One, 2012. **7**(11): p. e50262.
13. Davis, O.B., et al., *NPC1-mTORC1 Signaling Couples Cholesterol Sensing to Organelle Homeostasis and Is a Targetable Pathway in Niemann-Pick Type C*. Dev Cell, 2021. **56**(3): p. 260-276 e7.
14. Ullio, C., et al., *Sphingosine mediates TNFalpha-induced lysosomal membrane permeabilization and ensuing programmed cell death in hepatoma cells*. J Lipid Res, 2012. **53**(6): p. 1134-43.
15. Jimenez-Rojo, N., et al., *Membrane permeabilization induced by sphingosine: effect of negatively charged lipids*. Biophys J, 2014. **106**(12): p. 2577-84.
16. Carreira, A.C., R.F.M. de Almeida, and L.C. Silva, *Development of lysosome-mimicking vesicles to study the effect of abnormal accumulation of sphingosine on membrane properties*. Sci Rep, 2017. **7**(1): p. 3949.
17. Stahl-Meyer, J., K. Stahl-Meyer, and M. Jäättelä, *Control of mitosis, inflammation, and cell motility by limited leakage of lysosomes*. Curr Opin Cell Biol, 2021. **71**: p. 29-37.
18. Aits, S. and M. Jäättelä, *Lysosomal cell death at a glance*. J Cell Sci, 2013. **126**(Pt 9): p. 1905-1912.
19. Wang, F., R. Gomez-Sintes, and P. Boya, *Lysosomal membrane permeabilization and cell death*. Traffic, 2018. **19**(12): p. 918-931.
20. Maejima, I., et al., *Autophagy sequesters damaged lysosomes to control lysosomal biogenesis and kidney injury*. EMBO J, 2013. **32**(17): p. 2336-2347.
21. Hung, Y.H., et al., *Spatiotemporally controlled induction of autophagy-mediated lysosome turnover*. Nat Commun, 2013. **4**: p. ncomms3111.

22. Chauhan, S., et al., *TRIMs and Galectins Globally Cooperate and TRIM16 and Galectin-3 Co-direct Autophagy in Endomembrane Damage Homeostasis*. Dev Cell, 2016. **39**(1): p. 13-27.
23. Yoshida, Y., et al., *Ubiquitination of exposed glycoproteins by SCF(FBXO27) directs damaged lysosomes for autophagy*. Proc Natl Acad Sci, 2017. **114**(32): p. 8574-8579.
24. Papadopoulos, C. and H. Meyer, *Detection and Clearance of Damaged Lysosomes by the Endo-Lysosomal Damage Response and Lysophagy*. Curr Biol, 2017. **27**(24): p. R1330-R1341.
25. Skowrya, M.L., et al., *Triggered recruitment of ESCRT machinery promotes endolysosomal repair*. Science, 2018. **360**(6384): p. eaar5078.
26. Radulovic, M., et al., *ESCRT-mediated lysosome repair precedes lysophagy and promotes cell survival*. EMBO J, 2018. **37**(21): p. e99753.
27. Papadopoulos, C., B. Kravic, and H. Meyer, *Repair or lysophagy: dealing with damaged lysosomes*. J Mol Biol, 2020. **432**(1): p. 231-239.
28. Boye, T.L. and J. Nylandsted, *Annexins in plasma membrane repair*. Biol Chem, 2016. **397**(10): p. 961-969.
29. Koerdt, S.N., A.P.K. Ashraf, and V. Gerke, *Annexins and plasma membrane repair*. Curr Top Membr, 2019. **84**: p. 43-65.
30. Bendix, P.M., et al., *Interdisciplinary synergy to reveal mechanisms of annexin-mediated plasma membrane shaping and repair*. Cells, 2020. **9**(4): p. 1029.
31. Zhen, Y., et al., *Sealing holes in cellular membranes*. EMBO J, 2021. **40**: p. e106922.
32. Hurley, J.H., *ESCRTs are everywhere*. EMBO J, 2015. **34**(19): p. 2398-407.
33. McCullough, J., L.A. Colf, and W.I. Sundquist, *Membrane fission reactions of the mammalian ESCRT pathway*. Annu Rev Biochem, 2013. **82**: p. 663-92.

34. Pfitzner, A.K., et al., *An ESCRT-III Polymerization Sequence Drives Membrane Deformation and Fission*. Cell, 2020. **182**(5): p. 1140-1155 e18.
35. Pfitzner, A.K., J. Moser von Filseck, and A. Roux, *Principles of membrane remodeling by dynamic ESCRT-III polymers*. Trends Cell Biol, 2021. **31**(10): p. 856-868.
36. Bissig, C. and J. Gruenberg, *ALIX and the multivesicular endosome: ALIX in Wonderland*. Trends Cell Biol, 2014. **24**(1): p. 19-25.
37. Vietri, M., M. Radulovic, and H. Stenmark, *The many functions of ESCRTs*. Nat Rev Mol Cell Biol, 2020. **21**(1): p. 25-42.
38. Lizarbe, M.A., et al., *Annexin-phospholipid interactions. Functional implications*. Int J Mol Sci, 2013. **14**(2): p. 2652-2683.
39. Lennon, N.J., et al., *Dysferlin interacts with annexins A1 and A2 and mediates sarcolemmal wound-healing*. J Biol Chem, 2003. **278**(50): p. 50466-50473.
40. McNeil, A.K., et al., *Requirement for annexin A1 in plasma membrane repair*. J Biol Chem, 2006. **281**(46): p. 35202-35207.
41. Babiychuk, E.B., et al., *Blebbing confers resistance against cell lysis*. Cell Death Differ, 2011. **18**(1): p. 80-89.
42. Jaiswal, J.K., et al., *S100A11 is required for efficient plasma membrane repair and survival of invasive cancer cells*. Nat Commun, 2014. **5**: p. 3795.
43. Koerdt, S.N. and V. Gerke, *Annexin A2 is involved in Ca<sup>2+</sup>-dependent plasma membrane repair in primary human endothelial cells*. Biochim Biophys Acta Mol Cell Res, 2017. **1864**(6): p. 1046-1053.
44. Bittel, D.C., et al., *Annexin A2 mediates dysferlin accumulation and muscle cell membrane repair*. Cells, 2020. **9**(9): p. 1046-1053.
45. Boye, T.L., et al., *Annexin A4 and A6 induce membrane curvature and constriction during cell membrane repair*. Nat Commun, 2017. **8**(1): p. 1623.

46. Bouter, A., et al., *Annexin-A5 assembled into two-dimensional arrays promotes cell membrane repair*. Nat Commun, 2011. **2**: p. 270.
47. Demonbreun, A.R., et al., *An actin-dependent annexin complex mediates plasma membrane repair in muscle*. J Cell Biol, 2016. **213**(6): p. 705-718.
48. Swaggart, K.A., et al., *Annexin A6 modifies muscular dystrophy by mediating sarcolemmal repair*. Proc Natl Acad Sci, 2014. **111**(16): p. 6004-6009.
49. Demonbreun, A.R., et al., *Recombinant annexin A6 promotes membrane repair and protects against muscle injury*. J Clin Invest, 2019. **129**(11): p. 4657-4670.
50. Sonder, S.L., et al., *Annexin A7 is required for ESCRT III-mediated plasma membrane repair*. Sci Rep, 2019. **9**(1): p. 6726.
51. Jimenez, A.J., et al., *ESCRT machinery is required for plasma membrane repair*. Science, 2014. **343**(6174): p. science.1247136.
52. Scheffer, L.L., et al., *Mechanism of Ca<sup>2+</sup>-triggered ESCRT assembly and regulation of cell membrane repair*. Nat Commun, 2014. **5**: p. 5646.
53. Herbst, S., et al., *LRRK2 activation controls the repair of damaged endomembranes in macrophages*. EMBO J, 2020. **39**: p. e104494.
54. Scharf, B., et al., *Annexin A2 binds to endosomes following organelle destabilization by particulate wear debris*. Nat Commun, 2012. **3**: p. 755.
55. Jia, J., et al., *Galectin-3 coordinates a cellular system for lysosomal repair and removal*. Dev Cell, 2020. **52**(1): p. 69-87 e8.
56. Eapen, V.V., et al., *Quantitative proteomics reveals the selectivity of ubiquitin-binding autophagy receptors in the turnover of damaged lysosomes by lysophagy*. Elife, 2021. **10**: p. e72328.
57. Schindelin, J., et al., *Fiji: an open-source platform for biological-image analysis*. Nat Methods, 2012. **9**(7): p. 676-682.

58. Moss, S.E. and R.O. Morgan, *The annexins*. Genome Biol, 2004. **5**(4): p. 219.
59. Jacobson, L.S., et al., *Cathepsin-mediated necrosis controls the adaptive immune response by Th2 (T helper type 2)-associated adjuvants*. J Biol Chem, 2013. **288**(11): p. 7481-7491.
60. Kavcic, N., et al., *Intracellular cathepsin C levels determine sensitivity of cells to leucyl-leucine methyl ester-triggered apoptosis*. FEBS J, 2020. **287**(23): p. 5148-5166.
61. Bright, N.A., L.J. Davis, and J.P. Luzio, *Endolysosomes Are the Principal Intracellular Sites of Acid Hydrolase Activity*. Curr Biol, 2016. **26**(17): p. 2233-2245.
62. Repnik, U., et al., *L-leucyl-L-leucine methyl ester does not release cysteine cathepsins to the cytosol but inactivates them in transiently permeabilized lysosomes*. J Cell Sci, 2017. **130**(18): p. 3124-3140.
63. Rosengarth, A. and H. Luecke, *A calcium-driven conformational switch of the N-terminal and core domains of annexin A1*. J Mol Biol, 2003. **326**(5): p. 1317-1325.
64. Rosengarth A., L.H., *Annexin A2. Does it induce membrane aggregation by a new multimeric state of the protein?* Annexins, 2004. **1**(2): p. 129-136.
65. Shao, C., et al., *Crystallographic analysis of calcium-dependent heparin binding to annexin A2*. J Biol Chem, 2006. **281**(42): p. 31689-31695.
66. Rosengarth, A., et al., *Folding energetics of ligand binding proteins II. Cooperative binding of Ca<sup>2+</sup> to annexin I*. J Mol Biol, 2001. **306**(4): p. 825-35.
67. Jost, M., K. Weber, and V. Gerke, *Annexin II contains two types of Ca<sup>2+</sup>-binding sites*. Biochem J, 1994. **298 Pt 3**: p. 553-9.
68. Blackwood, R.A. and J.D. Ernst, *Characterization of Ca<sup>2+</sup>-dependent phospholipid binding, vesicle aggregation and membrane fusion by annexins*. Biochem J, 1990. **266**(1): p. 195-200.

69. Evans, T.C., Jr. and G.L. Nelsestuen, *Calcium and membrane-binding properties of monomeric and multimeric annexin II*. Biochemistry, 1994. **33**(45): p. 13231-13238.
70. de Araujo, M.E.G., et al., *Lysosomal size matters*. Traffic, 2020. **21**(1): p. 60-75.
71. Butor, C., et al., *Co-localization of hydrolytic enzymes with widely disparate pH optima: implications for the regulation of lysosomal pH*. J Cell Sci, 1995. **108**: p. 2213-2219.
72. Johnson, D.E., et al., *The position of lysosomes within the cell determines their luminal pH*. J Cell Biol, 2016. **212**(6): p. 677-692.
73. Abu-Remaileh, M., et al., *Lysosomal metabolomics reveals V-ATPase- and mTOR-dependent regulation of amino acid efflux from lysosomes*. Science, 2017. **358**(6364): p. 807-813.
74. Boye, T.L., et al., *Annexins induce curvature on free-edge membranes displaying distinct morphologies*. Sci Rep, 2018. **8**(1): p. 10309.
75. Roostalu, U. and U. Strahle, *In vivo imaging of molecular interactions at damaged sarcolemma*. Dev Cell, 2012. **22**(3): p. 515-29.
76. Drucker, P., et al., *Lipid segregation and membrane budding induced by the peripheral membrane binding protein annexin A2*. J Biol Chem, 2013. **288**(34): p. 24764-76.
77. Hakobyan, D., V. Gerke, and A. Heuer, *Modeling of annexin A2-Membrane interactions by molecular dynamics simulations*. PLoS One, 2017. **12**(9): p. e0185440.
78. de la Fuente, M. and A.V. Parra, *Vesicle aggregation by annexin I: role of a secondary membrane binding site*. Biochemistry, 1995. **34**(33): p. 10393-9.
79. Lambert, O., et al., *Structural analysis of junctions formed between lipid membranes and several annexins by cryo-electron microscopy*. J Mol Biol, 1997. **272**(1): p. 42-55.

80. Ayala-Sanmartin, J., P. Gouache, and J.P. Henry, *N-Terminal domain of annexin 2 regulates Ca(2+)-dependent membrane aggregation by the core domain: a site directed mutagenesis study*. Biochemistry, 2000. **39**(49): p. 15190-8.
81. Hu, N.J., et al., *Membrane-induced folding and structure of membrane-bound annexin A1 N-terminal peptides: implications for annexin-induced membrane aggregation*. Biophys J, 2008. **94**(5): p. 1773-81.
82. Eguchi, T., et al., *LRRK2 and its substrate Rab GTPases are sequentially targeted onto stressed lysosomes and maintain their homeostasis*. Proc Natl Acad Sci U S A, 2018. **115**(39): p. E9115-E9124.
83. Bonet-Ponce, L., et al., *LRRK2 mediates tubulation and vesicle sorting from lysosomes*. Sci Adv, 2020. **6**(46).
84. Ellison, C.J., et al., *Transbilayer Movement of Sphingomyelin Precedes Catastrophic Breakage of Enterobacteria-Containing Vacuoles*. Curr Biol, 2020. **30**(15): p. 2974-2983 e6.
85. Niekamp, P., et al., *Ca<sup>2+</sup>-activated sphingomyelin scrambling and turnover mediate ESCRT-independent lysosomal repair*. bioRxiv, 2021: p. 2021.03.12.435146.
86. Alonso, A. and F.M. Goni, *The Physical Properties of Ceramides in Membranes*. Annu Rev Biophys, 2018. **47**: p. 633-654.
87. Holopainen, J.M., M.I. Angelova, and P.K. Kinnunen, *Vectorial budding of vesicles by asymmetrical enzymatic formation of ceramide in giant liposomes*. Biophys J, 2000. **78**(2): p. 830-8.
88. Nurminen, T.A., et al., *Observation of topical catalysis by sphingomyelinase coupled to microspheres*. J Am Chem Soc, 2002. **124**(41): p. 12129-34.
89. Trajkovic, K., et al., *Ceramide triggers budding of exosome vesicles into multivesicular endosomes*. Science, 2008. **319**(5867): p. 1244-7.



90. Tam, C., et al., *Exocytosis of acid sphingomyelinase by wounded cells promotes endocytosis and plasma membrane repair*. J Cell Biol, 2010. **189**(6): p. 1027-38.
91. Babiychuk, E.B., et al., *The targeting of plasmalemmal ceramide to mitochondria during apoptosis*. PLoS One, 2011. **6**(8): p. e23706.
92. Babiychuk, E.B., K. Monastyrskaya, and A. Draeger, *Fluorescent annexin A1 reveals dynamics of ceramide platforms in living cells*. Traffic, 2008. **9**(10): p. 1757-75.
93. Jimenez, A.J. and F. Perez, *Physico-chemical and biological considerations for membrane wound evolution and repair in animal cells*. Seminars in Cell & Developmental Biology, 2015. **45**: p. 2-9.
94. Darwich, Z., et al., *Imaging lipid order changes in endosome membranes of live cells by using a Nile Red-based membrane probe*. RSC Advances, 2014. **4**(17): p. 8481-8488.
95. Zhanghao, K., et al., *High-dimensional super-resolution imaging reveals heterogeneity and dynamics of subcellular lipid membranes*. Nat Commun, 2020. **11**(1): p. 5890.
96. Goujon, A., et al., *Mechanosensitive Fluorescent Probes to Image Membrane Tension in Mitochondria, Endoplasmic Reticulum, and Lysosomes*. J Am Chem Soc, 2019. **141**(8): p. 3380-3384.
97. Rog, T., et al., *Ordering effects of cholesterol and its analogues*. Biochim Biophys Acta, 2009. **1788**(1): p. 97-121.
98. Punnonen, E.L., et al., *Intramembrane particles and filipin labelling on the membranes of autophagic vacuoles and lysosomes in mouse liver*. Cell Tissue Res, 1989. **258**(2): p. 269-76.
99. Kordylewski, L., T. Karrison, and E. Page, *P-face particle density of freeze-fractured vertebrate cardiac plasma membrane*. Am J Physiol, 1983. **245**(6): p. H992-7.
100. Chugh, P. and E.K. Paluch, *The actin cortex at a glance*. J Cell Sci, 2018. **131**(14).

101. Cabukusta, B. and J. Neefjes, *Mechanisms of lysosomal positioning and movement*. Traffic, 2018. **19**(10): p. 761-769.
102. Kazmierczak, Z., et al., *Endocytosis in cellular uptake of drug delivery vectors: Molecular aspects in drug development*. Bioorg Med Chem, 2020. **28**(18): p. 115556.
103. Serrano-Puebla, A. and P. Boya, *Lysosomal membrane permeabilization as a cell death mechanism in cancer cells*. Biochemical Society Transactions, 2018. **46**(2): p. 207-215.
104. Geisslinger, F., et al., *Targeting Lysosomes in Cancer as Promising Strategy to Overcome Chemoresistance-A Mini Review*. Front Oncol, 2020. **10**: p. 1156.

## **Acknowledgements**

I sincerely thank Noboru Mizushima and Hayashi Yamamoto for their generous mentorship, the Mizushima laboratory members for all their constructive comments and companionship, and my family (especially my Mother) and friends for their love and support. I am also grateful to the Japanese Ministry of Education, Culture, Sports, Science and Technology for providing me with a scholarship to pursue my graduate studies in Japan.